UNIVERSIDADE DO PORTO

FACULDADE DE ENGENHARIA

Master's Thesis

# Developing of a Gas Mixing System

Miguel Clare Neves

Supervisor: Prof. Dr. Ing. Abel Rouboa

Thesis submitted to Universidade do Porto – Faculdade de Engenharia
in partial fulfillment of the requirements for the degree of
Master in Mechanical Engineering - Fluids and Energy

MEM

U.PORTO

FEUP FACULDADE DE ENGENHARIA
UNIVERSIDADE DO PORTO

DEPARTAMENTO DE ENGENHARIA MECÂNICA
Faculdade de Engenharia

September, 2024

**Candidate:** Miguel Clare Neves, No. 201806627, up201806627@edu.fe.up.pt

**Scientific Guidance:** Prof. Dr. Ing. Abel Rouboa, rouboa@fe.up.pt

**Company:** Heilbronn University of Applied Sciences- Piston Machines Laboratory

**Advisor:** Prof. Dr. Ing. Karsten Wittek, karsten.wittek@hs-heilbronn.de

U.PORTO

FEUP FACULDADE DE ENGENHARIA
UNIVERSIDADE DO PORTO

DEPARTAMENTO DE ENGENHARIA MECÂNICA

Faculdade de Engenharia

Rua Dr. Roberto Frias, Porto

September, 2024

# Acknowledgements

I feel deeply grateful to my family for all the support they gave me during my work on this project.

To Prof. Abel Rouboa, thank you for making this experience possible, and to Prof. José Machado, for encouraging me to pursue a project abroad.

I'm grateful to Sebastian Biblioni, Bernardo Sotille, and Ítalo Basquera for all the time we spent together and the knowledge they shared with me.

To Ursulla Salwiczek, Thomas Schleeh, Geovane Prante, Vitor Cogo, and Alicia, many thanks for the warm welcome, for integrating me into the team, supporting this project and helping me expand my knowledge in ways I could never have expected.

To Prof. Karsten Wittek and Ana Ramos Wittek, I'm deeply thankful for the opportunity you gave me, the incredible experiences that allowed me to explore an exciting industry, and the unforgettable six months you provided.

# Abstract

The Fraunhofer-Gesellschaft Institute intends to analyze hydrogen production through the biomass gasification process characteristic of Germany. The gasification process produces a synthetic gas (Syngas) composed of Hydrogen, $H_2$, Carbon Monoxide, $CO$, Carbon Dioxide, $CO_2$, and Methane, $CH_4$. The content of each of these gases depends on various variables of the gasification process.

The context of this work involves a project that investigates to what extent Syngas needs to be filtered so that the gas performance in an *Internal Combustion Engine* (ICE) is equivalent to that obtained with pure hydrogen. Thus, it was necessary to develop a gas mixing system so that different mixtures and flow rates could be tested in an ICE at the *Kolbenmaschinen* Laboratory of the *Hochschule Heilbronn*.

The gas mixing system was developed by taking advantage of the compressibility of gases. In a compressible flow, if the ratio between the upstream pressure and the downstream pressure of an outlet section is less than the critical ratio, which depends on the isentropic index of each gas, the mass flow rate will only be a function of the upstream pressure and density and the area of the outlet section.

In this way, the mass flow rates of each of the gases in the mixture were calculated, considering that the engine operates at full load, which is the most critical scenario. We kept the upstream pressure at 30 *bar* and the downstream pressure between 12 and 15 *bar*, controlled through shut-off valves and a pressure gauge. Thus, we ensure that the pressure ratio remains below the critical ratio. Under these conditions, we calculated the orifice areas for the desired mass flow rate. A 100 $L$ tank was also introduced to stabilize the pressure in the system and minimize the number of start-ups and shutdowns.
Finally, three tests were conducted. The first was to obtain the discharge coefficient of the orifices, the second was to evaluate the operation of the gas mixing system, and the third was a test to compare pure *Hydrogen* ($H_2$) with a mixture of $CO_2$ and $H_2$ in the ICE.

**Keywords**: Hydrogen, Syngas, Internal Combustion Engine, Gas Mixing

# Resumo

O Instituto Fraunhofer-Gesellschaft pretende analisar a produção de hidrogénio através do processo de gaseificação de biomassa característica da Alemanha. O processo de gaseificação produz um gás sintético (Syngas) composto por Hidrogénio, $H_2$ , Monóxido de Carbono, $CO$, Dióxido de Carbono, $CO_2$, e Metano, $CH_4$. O teor de cada um destes gases depende de várias variáveis do processo de gaseificação.

O contexto deste trabalho insere-se num projeto queue pretende averiguar até que ponto o Syngas tem de ser filtrado para que o desempenho do gás num ICE ser equivalente ao obtido com hidrogénio puro. Assim, foi necessário desenvolver um sistema de mistura de gases de forma a que diferentes misturas e caudais possam ser testados em ICE no Labor *Kolbenmaschinen* da *Hochschule Heilbronn*.

O sistema de mistura de gases foi desenvolvido tirando vantagem da compressibilidade dos mesmos. Num escoamento compressível, se o rácio entre a pressão a montante e a pressão a jusante duma secção de saída for inferior ao rácio crítico, que depende do índice isentrópico de cada gás, o caudal mássico será apenas função da pressão e densidade a montate e da área da secção de saída.

Desta forma, foram calculados os caudais mássicos de cada um dos gases da mistura tendo em consideração que o motor opera em carga máxima, o cenário mais crítico. Mantivemos a pressão a montante a 30 *bar* e a pressão a jusante varia entre 12 e 15 *bar*, controlado através de válvulas de corte e de medidor de pressão. Assim, garantimos que o rácio de pressões se mantém sempre abaixo do rácio crítico. Com estas condições calculámos as áreas de orífico para o caudal mássico desejado. Foi também introduzido um tanque de 100 $L$ para estabilizar a pressão no sistema e minimizar o número de arranques e paragens do mesmo.

Por fim, foram realizados três testes. O primeiro para obter o coeficiente de descarga dos orifícios, um segundo para averiguar o funcionamento do sistema de mistura de gases e o terceiro teste para comparar o comportamento duma mistura de $H_2$ puro com uma mistura de $CO_2$ e $H_2$ num ICE.

**Palavras-Chave**: Hidrogénio, Syngas, Motor de Combustão Interna, Mistura de Gases

# Contents

**List of Figures** vii

**List of Tables** ix

**List of Acronyms** xi

**1 Introduction** 1
- 1.1 Project Background and Motivation . . . 1
- 1.2 Kolbenmaschinen Labor . . . 2
- 1.3 Project Objectives . . . 2
- 1.4 Structure . . . 3

**2 Literature Review** 5
- 2.1 Hydrogen . . . 5
- 2.2 Syngas . . . 11
- 2.3 Mixing Systems . . . 17

**3 Gas Mixing System Design** 21
- 3.1 Gas Compositions and Mass Flow Rates . . . 22
- 3.2 Dimensioning the Gas Mixing System . . . 25
- 3.3 Defining the Parts . . . 27
- 3.4 Gas Characterization . . . 30

**4 Experimental Investigation** 35
- 4.1 Internal Combustion Engine and Measurement Devices . . . 36
- 4.2 Calculation of Cd of the orifices . . . 38
- 4.3 Analysis of the Gas Measurement System . . . 39
- 4.4 Comparison between 100% $H_2$ and a mixture of $H_2$ and *Carbon Dioxide* ($CO_2$) . . . 41

**5 Conclusion** 45

**Appendix A Syngas Composition** 51

**Appendix B P&ID Plan** 53

**Appendix C Components Data Sheets** **55**
C.1 Pressure Regulator . . . . . 55
C.2 Shut-Off Valve . . . . . 56

**Appendix D Cantera Open-Source Codes** **57**
D.1 Cantera open-source code to calculate Adiabatic Flame Temperature . . . . 57
D.2 Cantera open-source code to calculate Laminar Flame Speed . . . . . 59
D.3 *EES* Code to Calculate Gas Properties . . . . . 61

**Appendix E ICE and Gas Mixing System Layout** **63**

# List of Figures


2.1 Outflow of compressible gas between 1 and 2 . . . . . 18
2.2 Variation of $\Psi$ (Top) and mass flow rate (Botton) with pressure ratio. . . . . 19

3.1 Time to fill the 100 *L* tank from 10 *bar* to 15 *bar*. . . . . 27
3.2 Various 3D models of the Gas Mixing System components. . . . . 29
3.3 Gax Mixing Unit components mounted in the existent infrastructure. . . . . 30
3.4 Computed adiabatic flame temperature for *Hydrogen* ($H_2$) and the three Synthesis Gas (Syngas)es. . . . . 31
3.5 Computed Minimum Ignition Energy (MIE) for $H_2$. . . . . 32

4.1 Old and new configurations of the pressure switches . . . . . 39
4.2 Behaviour of the Gas Mixing System. . . . . 41
4.3 Concentrations variations. Figure a): 75% and 25%, $H_2$ and *Carbon Dioxide* ($CO_2$), respectively. Figure b): 90% and 10%, $H_2$ and $CO_2$, respectively. 41
4.4 Behaviour of $H_2$ regulator with an orifice of 1.3 *mm*. . . . . 41
4.5 *Internal Combustion Engine* (ICE) performance comparison between 100% $H_2$ and 83% $H_2$ + 17% $CO_2$. . . . . 43

B.1 Gas Mixing System P&ID plan . . . . . 54

C.1 Pressure Reducer Specifications . . . . . 55
C.2 Shut-Off Valve Specifications . . . . . 56

E.1 Gas Mixing System and ICE Layout. . . . . 64
E.2 ICE mounted in the test cell. . . . . 65
E.3 Orifices and device used to test and calculate the Discharge Coefficient (Cd). 65

# List of Tables


2.1 Definitions of $H_2$ colour in Incer-Valverde, Korayem, Tsatsaronis, *et al.* [6] 6
2.2 $H_2$, *Methane* ($CH_4$) and Gasoline properties at 300$K$ and 101.315$kPa$ [2] . . 6
2.3 Mixture properties of $H_2$-Air, $CH_4$-Air and Gasoline-Air. Data given at 300 K and 1 atm (except the laminar burning velocity, given at 360 K and 1 atm) [2] . . . . . 7
2.4 Range for Syngas composition on a volume percent basis [14] . . . . . 11
2.5 Syngas elements properties from [7] . . . . . 12
2.6 Physicochemical properties of typical Syngas mixtures compared to other fuels [14] . . . . . 13
2.7 Volume compositions, in %, of the Syngas in table 2.6 . . . . . 13
2.8 Combustion properties with constant $\lambda$ from [19] . . . . . 15
2.9 Combustion properties varying $\lambda$ from [19] . . . . . 15
2.10 Critical conditions of different gases . . . . . 20

3.1 Syngas Volumetric Compositions Considered in Dimensioning the Gas Mixing System . . . . . 22
3.2 Gas Properties . . . . . 22
3.3 Mass fractions, $Y$, in % . . . . . 24
3.4 Calculated Properties . . . . . 24
3.5 Mass flow rates of each Syngas and element, in $kg/h$ . . . . . 25
3.6 Normalized flow rates for each element $i$ . . . . . 25
3.7 Orifices Calculation . . . . . 26
3.8 Orifices diameter in [mm] . . . . . 26
3.9 Lower Flammability Limit (LFL) calculations in %mol . . . . . 33
3.10 $\lambda$ values for ICE operation. . . . . 33

4.1 Technical data of the series 'TCD 3.6' from *Deutz* . . . . . 36
4.2 Theoretical orifices diameter calculation for 30 *bar* and 300 $K$ upstream of the nozzle. . . . . 38
4.3 Cd calculation for the orifice with 1.6 mm and 2 mm diameter. . . . . 38
4.4 Operation parameters with 100 % $H_2$ . . . . . 42
4.5 Operation parameters with 83 % $H_2$ and 17 % $CO_2$ . . . . . 42

A.1 Volumetric Composition of 3 Syngases obtained from different feedstocks . 51

# List of Acronyms

| | |
|---|---|
| $Ar$ | *Argon* |
| $CH_3OH$ | *methanol* |
| $CH_4$ | *Methane* |
| $CO$ | *Carbon Monoxide* |
| $CO_2$ | *Carbon Dioxide* |
| $H_2$ | *Hydrogen* |
| $H_2O$ | *Water* |
| $ISNO_x$ | Indicated Specific $NO_x$ |
| $NH_3$ | *Ammonia* |
| $NO_x$ | *Nitrogen Oxides* |
| $N_2$ | *Nitrogen* |
| $\chi$ | molar fraction |
| $(A/F)_s$ | stoichiometric mass air fuel ration |
| **Cd** | Discharge Coefficient |
| **CHP** | *Combined Heating and Power* |
| **CI** | *Compression Ignition* |
| **CNG** | *Compressed Natural Gas* |
| **CR** | *Compression Ratio* |
| **Cv** | Flow Coefficient |
| **DI** | *Direct Injection* |
| **DME** | *Dimethyl ether* |
| **EGR** | Exhaust Gas Recirculation |

| | |
|---|---|
| **EU** | *European Union* |
| **FC** | *Fuell Cell* |
| **ICE** | *Internal Combustion Engine* |
| **IMEP** | Indicated Mean Effective Pressure |
| **LFL** | Lower Flammability Limit |
| **LFS** | *Laminar Flame Speed* |
| **LHV** | *Low Heating Value* |
| **LPG** | Liquified petroleum gas |
| **MBT** | *Maximum Braque Torque* |
| **MEP** | *Mean Effective Pressure* |
| **MFB50** | *Mass Fraction Burned 50* |
| **MHV** | Mixture heating value |
| **MIE** | Minimum Ignition Energy |
| **MN** | *Methane Number* |
| **MON** | *Motor Octane Number* |
| **P&ID** | Piping and Instrumentation Plan |
| **PFI** | *Port Fuel Injection* |
| **R** | *Gas Constant* |
| **RPM** | *Rotations per minute* |
| **SBR** | *Steam-to-biomass ratio* |
| **SI** | *Spark Ignition* |
| **Syngas** | Synthesis Gas |
| **TDC** | *Top Dead Center* |
| **THC** | *Total Hydrocarbons* |
| **VGT** | Variable Geometry Turbine |
| **Y** | mass fraction |

# Chapter 1

# Introduction

## 1.1 Project Background and Motivation

The dissertation took place at the Piston Laboratory of the University of Applied Sciences of Heilbronn (*Labor Kolbenmaschinen, Hochschule Heilbronn*), under the supervision of Prof. Dr.-Ing Karsten Wittek.
It was part of a project of Fraunhofer Institute where they wanted to assess the viability of producing $H_2$, through the gasification of German biomass, filtrating the other molecules in the Syngas. They wanted to assess how much after-treatment the Syngas would have to have for the output of the unpurified $H_2$ in the ICE to be the same as of purified $H_2$.
Biomass gasification produces a Syngas containing $H_2$, $CO_2$, *Carbon Monoxide* ($CO$) and $CH_4$. Depending on several variables, such as gasification temperature, steam-to-biomass ratio, biomass feed rate and biomass type, it is possible to adjust the Syngas composition.
*Kolbenmaschinen Labor of Hochschule Heilbronn* will evaluate if the Syngas produced is appropriate for ICE use and suggest compositions of Syngas that may have the same output and operation parameters in an ICE as purified $H_2$. Furthermore, it would help Fraunhofer Institute determine the extent of treatment required for the Syngas to be suitable for ICEs operation.
The primary objective of the project is to develop and test a Gas Mixing System and test a mixture of $H_2$ and $CO_2$.

## 1.2 Kolbenmaschinen Labor

Piston Machine Laboratory (Kolbenmaschinen Labor) is part of the Applied Sciences University of Heilbronn, in the German State of Baden-Wurttemberg, 70 Km north of Stuttgart. The organization has four permanent employees and collaborates with major German automotive companies to develop new technologies. These projects provide students with opportunities to apply their acquired knowledge in practical settings.
Since 2018, the organization has shifted its focus to $H_2$-fueled ICE. They designed, developed, and self-financed their test cell for $H_2$ ICE. After completion, they did several studies and developed new technologies to enhance the use of $H_2$ in ICE making it their main topic of research. They are currently planning to construct two additional $H_2$ test cells, scheduled for completion by mid-2025.
At the end of this project, they will be able to test different mixtures of gases in ICE.

## 1.3 Project Objectives

This project is funded by the German Government and its a consortium of *Labor Kolbenmaschinen* of *Hochschule Heilbronn*, Fraunhofer Institute for Ceramic Technologies and Systems (*Fraunhofer-Institut für Keramische Technologien und Systeme IKTS*), Fraunhofer Institute for Environmental, Safety and Energy Technology-UMSICHT (*Fraunhofer-Institut für Umwelt-, Sicherheits- und Energietechnik UMSICHT*), and *DEUTZ Company*.
Fraunhofer-Institut UMSICHT researched and tested methods of production of Syngas obtained through different bio-residues typical from Germany such as Straw, Digestate and Sewage Sludge. It concluded that the gasification would be done at 750°C. Although other forms of production of Syngas, at different gasification parameters could produce a higher percentage of $H_2$, their goal was to choose a production method that would be feasible from an economical point of view.
Fraunhofer Institute for Ceramic Technologies and Systems developed a ceramic membrane to filter the Syngas components by their molecular size. This way, it is possible to filter the Syngas and only obtain the $H_2$ it produced. Furthermore, by using ceramic membranes to filter the gas, instead of chemical processes or different gasification parameters, we are reducing the production cost of $H_2$. However, it is unsure how purified the $H_2$ produced will be.
Thus, *Kolbenmaschinen Labor* needed to develop a Gas Mixing system and install it in their $H_2$ supply line to test different mixtures of $H_2$ with other molecules, such as $CO_2$, $CO$ and $CH_4$. Since the main goal is to power a $H_2$ ICE with the gas mixtures, the testing conditions were kept identical to those for $H_2$ fuel and the ICE remained unmodified. After the design and development of the Gas Mixing System, the performance of the Gas Mixing System was tested and a mixture of 83% $H_2$ and 17% $CO_2$ was tested in the ICE and compared with a mixture of 100% $H_2$. In the future, *Kolbenmaschinen Labor* will test the gas mixtures

provided by Fraunhofer-Institut UMSICHT and evaluate the gas compositions for a typical ICE operation as 100% $H_2$.
*DEUTZ Company* participates in the project as a partner, providing material for the tests.

## 1.4 Structure

Firstly, we examine why $H_2$ is being so discussed nowadays and how it is possible to convert an ICE into $H_2$ fueled ICE. Then we analyse the physical properties of the Syngas mixtures and what is being done to apply it to ICEs. Next, we see how other Laboratories mixed different gases to test them in ICEs. Afterwards, we discussed what parameters were considered to design the Gas Mixing System. Subsequently, the final design of the Gas Mixing System and the results of the tests conducted are shown. Finally, the results are analysed and compared with the $H_2$ ones and future works are proposed.

# Chapter 2

# Literature Review

## 2.1 Hydrogen

In 2020, the *European Union* (EU) announced a strategy to integrate $H_2$ into their Energy System. The strategy consists of 5 key areas: investment support, support production and demand, creating a hydrogen market and infrastructure, and research and international co-operation [1].
EU's interest in $H_2$ is a result of numerous factors, such as the volatile prices of fossil fuels, lack of energy security, worsening of global pollution and difficulty in the storage of electric energy, mainly from non-dispatchable energy sources [2][3][4][5]. Besides that, $H_2$ has some physical properties that make this element a great energy carrier, like its high energy density, abundance and availability [2]. $H_2$ can be employed in land, air and water vehicles as a fuel, not only for ICEs but also to *Fuell Cell* (FC) technology, which converts $H_2$ into *Water* ($H_2O$) and electricity [5]. It can also be used in residential heating, cooking, and electricity generation [5].

Various methods exist to produce $H_2$ each associated with a specific colour [6], as outlined in table 2.1. However, there is no consensus, yet, on how to characterize $H_2$, as some authors argue that 'green' $H_2$ refers to that produced from renewable electricity or biomass [6]. For this study, we define $H_2$ produced from biomass as 'green' $H_2$.

Table 2.1: Definitions of $H_2$ colour in Incer-Valverde, Korayem, Tsatsaronis, *et al.* [6]

| Color | Source of Energy | Source of $H_2$ | Production Process | $CO_2$ emissions |
|---|---|---|---|---|
| Green | Renewable Energy | Water | Electrolysis | No direct $CO_2$ emission |
| Orange | Mix of electricity grid | Water | Electrolysis | Depends on the electricity mix |
| Pink | Nuclear | Water | Electrolysis | No direct $CO_2$ emissions |
| Red | Nuclear | Water | Thermolysis/ Thermochemical process | No direct $CO_2$ emissions |
| Gray | Electricity from non-renewable | Natural Gas | Steam Methane Reforming | High |
| Blue | Electricity from non-renewable | Natural Gas/ Biomass | Steam Methane Reforming | Low |
| Turquoise | Electricity from non-renewable | Natural Gas | Pyrolysis | No direct $CO_2$ emissions |
| Brown | Electricity from non-renewable | Lignite coal/ Biomass | Gasification | High |
| Black | Electricity from non-renewable | Bituminous coal | Gasification | High |

Table 2.2: $H_2$, $CH_4$ and Gasoline properties at $300K$ and $101.315kPa$ [2]

| Property | $H_2$ | $CH_4$ | Gasoline |
|---|---|---|---|
| Molecular Weight $[g/mol]$ | 2.016 | 16.043 | 114.236 |
| Specific Mass $[kg/m^3]$ | 0.08 | 0.65 | 692 |
| Mass Diffusivity in Air $[cm^2/s]$ | 0.61 | 0.16 | 0.07 |
| Minimum Ignition Energy $[mJ]$ | 0.02 | 0.28 | 0.28 |
| Minimum Quenching Distance $[mm]$ | 0.64 | 2.03 | 3.5 |
| Flammability Limits $[\lambda]$ | 10-0.14 | 2-0.6 | 1.51-0.26 |
| *Low Heating Value* (LHV) $[MJ/kg]$ | 120 | 50 | 44.3 |
| Stoichiometric Air-to-Fuel Ratio $[kg/kg]$ | 34.2 | 17.1 | 15.0 |

### $H_2$ Properties and Application to ICE

Important physical properties of $H_2$ can be seen in table 2.2, compared with $CH_4$ and Gasoline, all data given at 300 $K$ and 101.315 $kPa$ from Verhelst and Wallner [2]. Through Mass Diffusivity it can be seen that $H_2$ can spread much faster in the air than $CH_4$ and Gasoline. Regarding ignition, $H_2$ requires significantly less energy to ignite compared to other substances—approximately one order of magnitude less [2]. However, this energy measurement is conducted using a capacitive charge-discharge, making it dependent on the spark gap, a smaller spark gap results in a lower minimum ignition energy. Additionally, the ignition energy depends on the air-to-fuel mass ratio [2]. Since $H_2$ has a lower minimum ignition energy, its flammability limits are more spread than the two other fuels which allow a wide range of engine power output through the change in the mixture equivalence ratio [2]. $H_2$ lower heating value is much higher than $CH_4$ and Gasoline because $H_2$ product of combustion is only $H_2O$, making it able to store much more energy per kilogram than the other two [2]. However, $H_2$ requires a significantly higher amount of air for a stoichiometric burn [2]. Table 2.3 compares $H_2$-air stoichiometric and lean mixtures with $CH_4$-air and gasoline-air stoichiometric mixtures. Verhelst and Wallner [2] conducted an in-depth review on the application of $H_2$ in ICEs. Its high auto-ignition temperature indicates it's better employed in *Spark Ignition* (SI) engines than in *Compression Ignition* (CI) engines. Since it has a wider range of flammability limits it allows for a qualitative control, instead of quantitative control. Quantitative control is when the air-fuel mass ratio is kept constant, while qualitative control is when the mixture richness is changed at wide open throttle, varying only the mass of fuel injected [7]. Despite its high gravimetric LHV, $H_2$

has lower specific mass compared to other fuels, as can be seen in table 2.2, which is reflected in its volumetric energy content. Although the heating values differ, the Mixture heating value (MHV) for different fuels at stoichiometric conditions are of the same magnitude. This is important because it means that the performance achieved with an engine using different fuels is approximately the same [8]. Because of its low specific mass, a large air charge displacement is required, reducing the mixture energy density introduced per working cycle, thus reducing the engine's power density [9]. This can be overcome by introducing a turbocharging system [10]. Furthermore, $H_2$ has a significantly higher laminar burning velocity, despite being a major quality of the gas, it enhances abnormal combustion at stoichiometric conditions, such as autoignition, surface ignition and backfiring [2]. In abnormal combustion, hot surfaces in the combustion chamber can ignite the fuel-air mixture prematurely [7]. Pre-ignition generally describes combustion events inside the combustion chamber during the engine compression stroke, with the actual start of combustion before spark timing [2]. Backfiring refers to events where the air-fuel mixture combusts during the intake stroke, usually in an intake runner or intake manifold. Engine 'knock' is the term used to describe the autoignition of the remaining end-gas during the late part of the combustion event, resulting in high-pressure oscillation [2], in SI engines. It's important to avoid this phenomenon because when two flame fronts coexist in the combustion chamber, their collision creates an enormous pressure wave that may damage the engine [7]. All these phenomena are enhanced with $H_2$ high adiabatic flame temperature at stoichiometric conditions [2]. Furthermore, it also increases the presence of *Nitrogen Oxides* ($NO_x$) in the exhaust gases [11]. To prevent these phenomena and to compile with EU's regulation in emissions of $NO_x$, a homogeneous lean-burn strategy is suggested, taking advantage of $H_2$ wide flammability limits [2][12].

Table 2.3: Mixture properties of $H_2$-Air, $CH_4$-Air and Gasoline-Air. Data given at 300 K and 1 atm (except the laminar burning velocity, given at 360 K and 1 atm) [2]

| Property | $H_2$-Air $\lambda = 1$ | $H_2$-Air $\lambda = 4$ | $CH_4$-Air $\lambda = 1$ | Gasoline-Air $\lambda = 1$ |
|---|---|---|---|---|
| Volume fraction fuel [%] | 29.5 | 9.5 | 9.5 | 1.65 |
| Mixture density [$kg/m^3$] | 0.85 | 1.068 | 1.123 | 1.229 |
| Autoignition Temperature [$K$] | 858 | >858 | 813 | 690 |
| Adiabatic Flame Temperature [$K$] | 2390 | 1061 | 2226 | 2276 |
| Air-to-fuel ratio [$kg/kg$] | 34.2 | 136.6 | 17.1 | 15.1 |
| Laminar flame speed[$cm/s$] | 290 | 12 | 48 | 45 |
| Gravimetric energy content [$kJ/kg$] | 3758 | 959 | 3028 | 3013 |
| Volumetric energy content [$kJ/m^3$] | 3189 | 1024 | 3041 | 3704 |

The desire to prevent combustion anomalies discussed previously has led to most of the measures suggested to convert diesel or gasoline ICEs into $H_2$ICEs [2]. Accordingly to

Verhelst and Wallner [2], $H_2$ ICE modifications needed are:

- Spark plugs: cold-rated spark plugs avoid electrode temperatures exceeding the auto-ignition temperatures. Spark plugs with platinum electrodes can be a catalyst for hydrogen oxidation, which is to be avoided.
- Ignition system: high voltage output ignition system is recommended, as the ignition of $H_2$ mixtures need a second ignition voltage due to a lower ion concentration of the $H_2$ flame.
- Injection system: two methods can be used, *Port Fuel Injection* (PFI) or *Direct Injection* (DI):
  - PFI is when fuel is injected in the intake air manifold, just before the intake valve [7]. Regarding $H_2$, the high flow requirements can be mitigated by using multiple injectors.
  - DI is when fuel is injected directly into the combustion chamber, during the compression stroke [7]. Concerning $H_2$, it is needed high flow rate injectors with instantaneous flows around 4-6 $g/s$ at $10^5$ $kPa$ supply pressure.
- *Compression Ratio* (CR): should be as high as the fuel allows, the limit is established when high heat losses and combustion anomalies start to occur. $H_2$ ICEs compression ratio various between 7.5:1 and 14.5:1.

**$H_2$ Internal Combustion Engine**

Wittek, Cogo, and Prante [13] developed an in-depth study on optimizing a $H_2$ ICE with a converted industrial diesel engine. Firstly, without any modifications, the engine was run with diesel for baseline results to be compared with the results with $H_2$. Before running with $H_2$ they did the following modifications:

- Reduction of the geometric CR, from 17.2:1 to 10:1,
- Application of an ignition system, with cold-rated spark plugs and a prototype ignition coil,
- Application of a gas injection system, PFI injectors originally designed for gaseous fuels such as compressed natural gas and liquified petroleum gas.

Following, they also conducted a baseline test for $H_2$ combustion, without any optimization and compared the results with the diesel baseline tests. They reached the following conclusions:

- The operation strategy applied that was not optimized has seen the efficiency levels in larger parts of the map only slightly lower than the diesel engine, which is remarkable since lower CR in the $H_2$ engine,

- The $NO_x$ emissions increased at high loads with a steep gradient. The full load torque that can be displayed results from the target value set for the emissions, which was 5 $g/kWh$,
- Under these conditions, the $H_2$ engine does not achieve the full load torque behaviour of the diesel engine and, at speeds below 1400 $min^{-1}$, a significant gap can be seen.

To improve the trade-off of $NO_x$ emissions and torque output and simplify the system (without the application of exhaust gas treatment), they tested three different approaches with the boundary condition of Indicated Specific $NO_x$ ($ISNO_x$) emissions to be below 1 $g/kWh$:

1. Variation of the Wastegaste Turbocharger spring load, that limits the intake manifold absolute pressure at high loads. The spark timing was adjusted to 50 % *Mass Fraction Burned 50* (MFB50) at 8 *dCA ATDC* and Exhaust Gas Recirculation (EGR) was not introduced in these tests. As the WG Pre-load was increased, higher boost levels could be achieved, without the need to enrichening the mixture at higher loads, decreasing the $NO_x$ emissions and improving the thermal efficiency because of lower heat transfer losses. Comparing the setup with the original spring setting with the one with maximum preload, the maximum operable Indicated Mean Effective Pressure (IMEP) was increased from 14 *bar* to 16.5 *bar* while the $NO_x$ emissions stayed below the mentioned value,
2. Variation of the spark timing, as the combustion is delayed, the in-cylinder peak pressure will be lower, as the combustion temperature, resulting in lower $NO_x$ production rates. A spark sweep was performed at 1600 $min^{-1}$ and constant fuel injection duration. No EGR was employed and the Wastegate Turbocharger was used with the higher spring preload. With delaying spark-timing a continuous drop in IMEP was seen, due to lower peak pressure in the cylinder, which translates into a reduction of the expansion work, affecting the thermal efficiency. Considering the $ISNO_x$limit, an IMEP of 18.7 *bar* was obtained with a centre of combustion at 14 *dCA ATDC*,
3. Application of high pressure EGR, with the same turbocharger setup as the previous test, at 1600 $min^{-1}$ but with the EGR valve fully open and no intake throttling. At the lower load the intake manifold absolute pressure was almost not affected by the EGR, while $\lambda$ drops continuously towards lower loads with EGR. As a result of the increase of the inert mass, lower combustion temperatures were reached, which resulted in a reduction of the $ISNO_x$ emissions and an increase in thermal efficiency due to lower combustion temperatures and reduction of heat transfer losses.
4. Finally, the three measures described were applied across the entire speed range. The maximum spring pre-load was applied and the EGR was only applied at a speed equal to or greater than 1600 $min^{-1}$. A full-load operating point was optimized iteratively at each engine speed. For that purpose, the injected fuel mass was increased stepwise

and the ignition was retarded after each step until the $NO_x$ emissions matched the limit value. A significant increase of IMEP can be seen between 1400 $min^{-1}$ and 2000 $min^{-1}$ while complying with the set limit of emissions imposed. However, significant efficiency losses arise due to the spark ignition delay. At higher speeds, there is enough enthalpy flow for the turbine so high pressure EGR can be employed. Its application allows for a reduction of the need for spark retardation. They concluded that a noteworthy increase of the full load IMEP curve was achieved, while two weak points were not surpassed, the significant gap to full load at low engine speeds (bellow 1400 $min^{-1}$) and a significant loss of efficiency over a wide speed range.

To overcome this problem they applied a Variable Geometry Turbine (VGT) instead of the wastegate turbocharger. It enables maximum energy extraction at the whole engine speed range and can help mitigate both of the problems mentioned above. They provide a new degree of freedom, the position of the guide vanes, and allow the VGT to have behaviours like smaller or bigger turbines. A full load operating point was optimized iteratively at each engine speed in the same manner described in the previous test. High pressure EGR was only employed at speed equal to or above 1600 $min^{-1}$. Both turbochargers enable a comparable torque output at speeds above 1400 $min^{-1}$. Towards the end of the speed range, VGT provides slightly more torque. Bellow 1400 $min^{-1}$ both $H_2$ full load curves fall behind the diesel baseline curve, with the VGT drawing more torque output at those speeds than the wastegate turbocharger since it needs less spark retardation to comply with the $NO_x$ limit and it leads to higher thermal efficiency. The same $NO_x$ reduction was achieved with both turbochargers, however, the VGT has less efficiency drawback.
They determined that converting a diesel engine to run on hydrogen can achieve a nearly emission-free propulsion system while maintaining a large number of the operating characteristics of the diesel engine.
Their work shows that is possible to convert a diesel engine to $H_2$ without the need for many modifications while maintaining the emissions level below the legislated. At low speeds, the torque output is below the diesel one. However, at higher speeds the $H_2$ engine achieved higher torque outputs.

## 2.2 Syngas

Syngas is formed by a gasification process from natural gas, heavy oil, biomass or coal. A complex and long chain of events converts the feed into simpler molecules, such as $H_2$, $CH_4$, $CO_2$, $CO$, $H_2O$ and *Nitrogen* ($N_2$) [14]. Depending on the process adopted for gasification, its parameters and the feedstock used, the Syngas will have varying compositions and heating values [14]. The best compositions generally depend upon the usage of Syngas, feedstock and production costs [14]. A possible range for Syngas composition on a volume per cent basis can be seen in table 2.4.

Table 2.4: Range for Syngas composition on a volume percent basis [14]

| Species | Min | Max |
|---|---|---|
| $H_2$ | 8.6 | 61.9 |
| $CO$ | 22.3 | 55.4 |
| $CH_4$ | 0.0 | 8.2 |
| $CO_2$ | 1.6 | 30.0 |
| $H_2O$ | - | 39.8 |
| $N_2$+*Argon* ($Ar$) | 0.2 | 49.3 |
| LHV [$MJ/m^3$] | 5.02 | 12.57 |

Syngas can be an intermediate to other clean fuels such as *Ammonia* ($NH_3$), *Dimethyl ether* (DME) or *methanol* ($CH_3OH$) [14]. Some of the applications of Syngas are [14]:

- Power generation in existing coal power plants.
- *Combined Heating and Power* (CHP) plants. ETTES [15] has done extensive studies on the application of Syngas in CHP plants. They produce Gensets that can work with a broad range of Syngas compositions.
- Integrated gasification combined cycles.
- Fuel cells.
- Gas turbines.
- Green $H_2$ production [3].
- Directly as the primary or secondary fuel in ICEs:
  - As dual-fuel in CI engines, with diesel [16].
  - As fuel in homogenous charge SI [16] engines and DI engines [16][17].

As stated before, Syngas is produced through the gasification of coal, biomass or waste into a high-temperature environment, in which the controlled operating conditions and the oxygen deficiency induce partial oxidation of the feedstock, producing Syngas [16] The

feedstock is in contact with a gasifying agent like oxygen, steam or air [14].
Syngas composition depends on which gasifier agent is used [16][14], on which feedstock is used [16][14], of the gasifier layout and operating conditions [16]. Martins, Rouboa, and Monteiro [3] conducted a study on the techno-economic viability of green $H_2$ production through different gasification processes. They simulated the green $H_2$ production through three different types of gasifications: conventional biomass gasification, plasma biomass gasification and supercritical water gasification. It is shown that the $H_2$ yield depends on the gasification temperature, the feed concentration and the *Steam-to-biomass ratio* (SBR). Important ICEs manufacturers produce engines that can run on Syngas such as *Caterpillar* and *Edina*. Both companies produce these engines to operate in CHP power plants at 1500 *Rotations per minute* (RPM). Based on their size, they can produce between 400 and 4000 $kW$. As previously mentioned, ETTES [15] have pilot CHP power plants running on Syngas, where they adapted ICEs from different manufacturers to Syngas. However, it was not clear what modifications were made to ensure successful operation on Syngas.

**Syngas Properties**

Properties of Syngas are highly variable due to the numerous possible combinations of its composition. Table 2.5 shows some physical properties of the typical Syngas elements. Its properties are a function of the mass composition of the gas and its variation can be seen in tables 2.6 and 2.7.

Table 2.5: Syngas elements properties from [7]

| Element | Molecular Weight $g/mol$ | Specific mass[1] $kg/m^3$ | LHV $MJ/kg$ | $(A/F)_s$ |
|---|---|---|---|---|
| $H_2$ | 2.02 | 0.09 | 120.0 | 34.3 |
| $CO$ | 28.01 | 1.25 | 10.1 | 2.47 |
| $CH_4$ | 16.04 | 0.72 | 50 | 17.23 |
| $CO_2$ | 44.01 | 1.96 | - | - |

Paykani, Chehrmonavari, Tsolakis, *et al.* [14] conducted a in-depth review of the application of Syngas to ICEs. Table 2.6 shows various physicochemical properties of different mixtures of Syngas compared with $H_2$, $CH_4$, biogas and conventional fossil fuels. Table 2.7 shows the volume compositions of the gases in table 2.6.

Some chemical properties, such as auto-ignition temperature, adiabatic flame temperature, *Laminar Flame Speed* (LFS), minimum ignition energy, quenching distance, etc. are hard to extrapolate or to model since they depend on multiple variables [14]. These are key properties to characterize the combustion of Syngas and to determine possible modifications in ICEs. Its high LFS and wide flammability limits than traditional fuels are due to the

[1] At T=273.15 $K$ and P=101.325 k$Pa$.
[2] All properties at T=298.15 $K$ and P=101.325 k$Pa$.
[3] At stoichiometric conditions.

Table 2.6: Physicochemical properties of typical Syngas mixtures compared to other fuels [14]

| Properties[2] | Syngas 1 | Syngas 2 | Syngas 3 | Syngas 4 | Syngas 5 | Biogas | $H_2$ | $CO$ | $CH_4$ | Gasoline | Diesel |
|---|---|---|---|---|---|---|---|---|---|---|---|
| Specific Mass $[kg/m^3]$ | 0.54 | 0.67 | 0.68 | 1.05 | 1.04 | 1.11 | 0.0824 | 1.145 | 0.656 | 719.7 | 832 |
| Molecular weight $[kg/mol]$ | 13.91 | 15 | 15.2 | | 23.2 | 34.4 | 2.0 | 28 | 16.04 | 103 | 200 |
| Stoichiometric Air-to-Fuel Ratio $[kg/kg]$ | 5.3 | 4.58 | 7.23 | 1.4 | 2.07 | 5.67 | 34.2 | 2.5 | 17.2 | 14.7 | 14.7 |
| Flammability Limits [vol% in air] | 24-60 | 6.06-74.2 | 5.8-41.4 | 7-21.6 | 13.4-58 | 7.5-14 | 4-75 | 12.5-74 | 5-15 | 1.4-7.6 | 0.6-7.5 |
| Auto-ignition temperature $[K]$ | 980 | 873-923 | 873-923 | 898 | 898 | 923 | 858 | 882 | 813 | 550 | 589 |
| Minimum Ignition Energy $[mJ]$[3] | - | - | - | - | - | - | 0.02 | - | 0.28 | 0.24 | - |
| Laminar flame speed $[cm/s]$[3] | 100 | 180 | - | 50 | 50 | 25 | 180-280 | 40 | 38 | 37-43 | - |
| Adiabatic flame temperature $[K]$[3] | 2584 | 2385 | 2400 | - | 2200 | 2145 | 2390 | 2214 | 2214 | 2580 | - |
| Quenching Distance $[mm]$[3] | - | - | - | - | - | - | 0.64 | 1.6 | 2.1 | 2.84 | - |
| Low heating value $[MJ/kg]$ | 15.7 | 17.54 | 24.4 | 5 | 7.47 | 17.0 | 119.7 | 10.1 | 50.0 | 43.4 | 42.6 |
| Volumetric energy content $[MJ/m^3]$ | 8.47 | 11.75 | 16.59 | 5.25 | 7.84 | 18.87 | 9.86 | 11.56 | 32.8 | 31235 | 35443 |

Table 2.7: Volume compositions, in %, of the Syngas in table 2.6

| Element | Syngas 1 | Syngas 2 | Syngas 3 | Syngas 4 | Syngas 5 | Biogas |
|---|---|---|---|---|---|---|
| $H_2$ | 57 | 50 | 40 | 22.6 | 19.6 | - |
| $CO_2$ | - | - | - | 9.3 | 5.42 | 42.3 |
| $CO$ | 43 | 50 | 40 | 24.3 | 29.6 | - |
| $CH_4$ | - | - | 20 | 2.2 | 5.27 | 55.6 |
| $N_2$ | - | - | - | - | 40.56 | 2.1 |

high percentage of $H_2$, which means that a lean-burning strategy may be employed [14]. No available data for minimum ignition energy hinders the ignition system's characterisation. However, the $H_2$ content can facilitate cold starts and guarantee quick ignition.

In Paykani, Chehrmonavari, Tsolakis, *et al.* [14] review they also conducted an in-depth analysis of how different elements affect some of the previously mentioned characteristics. Adding $CO$ will increase the flame instability. Increasing $CO_2$ inhibits LFS due to its direct role in chemical reactions. Increasing $CH_4$ leads the LFS peak to move towards the lean side and will significantly reduce the LFS due to slower LFS of $CH_4$. However, few experimental data are available for the LFS of Syngas with $CH_4$. It was concluded that measuring LFS of high content $H_2$ Syngas at high pressure with reasonable accuracy was extremely difficult because significant differences between experimental and modelled data were found, which was attributed to uncertainty in key reactions.

An important parameter for gaseous fuel application in ICE is the *Methane Number* (MN) which indicates the fuel propensity to resist knock. Its equivalent for liquid fuels is the *Motor Octane Number* (MON). The MN rating system utilizes a reference fuel blend of $CH_4$ and $H_2$, where $CH_4$ is assigned an MN of 100 and $H_2$ is assigned an MN of zero. Additionally, $CH_4$-$CO_2$ mixtures are considered reference mixtures for MN values above 100, where the MN is defined as 100 plus the volume percentage of $CO_2$ present. For instance, a mixture of 20% $CO_2$ and 80% $CH_4$ (by volume) results in an MN of 120, while a mixture of 20% $H_2$ and 80% $CH_4$ (by volume) leads to an MN of 80. Consequently, an engine fueled with Syngas that has a higher $CO_2$ content is expected to have an increased upper limit for the CR without experiencing knock [14]. More generally, once the MN value is determined using this method, adjusting both the spark timing and the CR can be used to prevent knock. The procedure for specifying the MN of tested fuel is a comparative basis

in which unknown fuel is indirectly compared to a map of reference blends at the same CR via a curve. Some researchers have conducted procedures to evaluate the MN for a certain gas mixture through simulation models and extrapolation of available data. However, it was found that these estimates deviate considerably from experimental data when Syngas is considered as fuel because some of the models developed do not consider the effect of $CO$ nor $CO_2$. Paykani, Chehrmonavari, Tsolakis, *et al.* [14] concluded that there isn't a comprehensive consensus to determine the knock propensity of gaseous fuels. Through tests conducted by Lechner, Hornung, and Brautsch [18] it was concluded that all Syngas blends were more prone to knock than $CH_4$ or biogas. Through Paykani, Chehrmonavari, Tsolakis, *et al.* [14] definition of MN, we can assume that adding $CO_2$ and $CH_4$ to the mixture will reduce the knocking tendency of the gas. This is important because if a mixture of $H_2$, $CO_2$ and $CH_4$ has more knocking resistance than only $H_2$, the CR can be higher and a better efficiency can be achieved.
The minimum ignition energy is calculated through the following equation [11]:

$$E_{ign} = 61.6P(\frac{c_p}{R_b})(\frac{T_b - T_u}{T_b})(\frac{\alpha}{S_L})^3, \tag{2.1}$$

- P represents pressure, in Pa.
- $R_b$ is the universal gas constant divided by the molecular weight of the burned gases, in $kJ/\text{k}molK$.
- $c_p$ is the average specific heat at constant pressure of the gas-air mixture, between $T_b$ and $T_u$ in $kJ/kgK$.
- $T_b$ is the adiabatic temperature of the fuel-air mixture, in $K$.
- $T_u$ is the initial temperature of the gas-air mixture, in $K$.
- $\alpha$ is the thermal diffusivity of the gas-air mixture, in $m^2/s$.
- $S_L$ is the LFS in m/$s$.

Equation 2.1 shows that minimum ignition energy depends on multiple variables. Regarding Syngas, little to no information was found about this parameter. This can be explained by the conclusion by Paykani, Chehrmonavari, Tsolakis, *et al.* [14] that is very difficult to accurately measure the LFS of high $H_2$ content Syngas. This lack of information makes it difficult to characterize the ignition system accurately. Furthermore, flammability limits are obtained through the cubic limits of the minimum ignition energy varying the air-to-fuel ratio. Without this parameter, it is also difficult to understand in which air-to-fuel ratios the gas should operate.

**Syngas in ICE**

Bika [19] conducted tests with Syngas mixtures of 50% $H_2$ 50% $CO$ and 75% $H_2$ 25% $CO$. He concluded that an increment of $CO$ increases the knock limit and the combustion duration of the Syngas. It used a single cylinder able to vary CR from 4:1 to 18:1 during operation, with PFI. However, there was no mention to the inlet pressure of the charge. They modified the original configuration to accommodate electronic gaseous fuel injection and spark timing control. Table 2.8 shows a summary of the results obtained with constant $\lambda$ while table 2.9 shows a summary of the results obtained with varying $\lambda$ and constant CR.

Table 2.8: Combustion properties with constant $\lambda$ from [19]

| $H_2/CO$ | $\lambda$ | CR | Spark Timing | Indicated Efficiency | CA10 | MFB50 | CA90 |
|---|---|---|---|---|---|---|---|
| 100% | 1.66 | 6 | -9 | 28.4% | 5.4 | 14.4 | 27.7 |
| 75% | 1.66 | 6 | -13 | 28.7% | 4.7 | 14.8 | 29.2 |
| 50% | 1.66 | 6 | -17 | 28.8% | 5 | 16.2 | 29.9 |
| 100% | 1.66 | 8 | -7 | 30.3% | 3.2 | 13.3 | 20.2 |
| 75% | 1.66 | 8 | -11 | 30.4% | 2.2 | 13.3 | 20.5 |
| 50% | 1.66 | 8 | -17 | 30.7% | -1.1 | 11.5 | 19.8 |
| 100% | 1.66 | 10 | -7 | 31.5% | 1.1 | 11.5 | 18.0 |
| 75% | 1.66 | 10 | -11 | 31.5% | -1.8 | 10.8 | 18.0 |
| 50% | 1.66 | 10 | -16 | 32% | -4.7 | 9.7 | 18.0 |

Table 2.9: Combustion properties varying $\lambda$ from [19]

| $H_2/CO$ | $\lambda$ | CR | Spark Timing | Indicated Efficiency | CA10 | MFB50 | CA90 |
|---|---|---|---|---|---|---|---|
| 100% | 1.66 | 6 | -9 | 28.4% | 5.4 | 14.4 | 27.7 |
| 75% | 1.66 | 6 | -13 | 28.7% | 4.7 | 14.8 | 29.2 |
| 50% | 1.66 | 6 | -17 | 28.8% | 5 | 16.2 | 29.9 |
| 100% | 1.43 | 6 | -5 | 27.6% | 5 | 12.2 | 27.7 |
| 75% | 1.43 | 6 | -9 | 27.5% | 5 | 12.2 | 28.8 |
| 50% | 1.43 | 6 | -13 | 27.6% | 4 | 13.3 | 29.5 |
| 100% | 1.25 | 6 | -1 | 26.2% | 4 | 11.9 | 27.0 |
| 75% | 1.25 | 6 | -3 | 26.3% | 6.5 | 14 | 28.4 |
| 50% | 1.25 | 6 | -9 | 26.7% | 7.2 | 13.3 | 30.2 |

Spark timing represents the crank degree angle relative to the *Top Dead Center* (TDC), where *Maximum Braque Torque* (MBT) is achieved. Indicated efficiency is the ratio of work transferred to the piston from the in-cylinder fuel chemical energy [7]. MFB50 is the crank angle where 50% of the mass fraction is burned [7]. MFB5010 and MFB5090 represents the crank angle where 10% and 90% mass of the fuel is burned, respectively [7]. The difference between the two is the combustion duration, in crank angle.

Hagos, Aziz, and Sulaiman [17] did an experimental study on the combustion, performance and emissions of Syngas on a DI SI engine. He validated the wide range of operation of the

Syngas. However, other combustion and performance parameters lacked operation information, such as the air-to-fuel ratio, which made it difficult to evaluate the results. Furthermore, no information was given about the engine modifications/specifications for Syngas operation. He compared the results with *Compressed Natural Gas* (CNG). Syngas showed a higher peak cylinder pressure, higher heat release rate and faster combustion, at all operation speeds and loads. Lower $CO$ emissions were observed at higher loads but increased at lower loads. $NO_x$ emission was higher at all load and speed conditions. *Total Hydrocarbons* (THC) emission improved significantly at all engine loads and speeds. However, we cannot accurately evaluate these conclusions since they did not clarify the operation parameters of the test. Through the experimental setup schematics it can be assumed that the ICE used is naturally aspirated.

Fiore, Magi, and Viggiano [16] stated that the most important emissions in Syngas combustion are limited to $NO_x$ and $CO$. The last is related to the Syngas $CO$ content while $NO_x$ are associated with engine geometry and its operating parameters. Its significant emission may be related to its high flame speed and high combustion temperature.

## 2.3 Mixing Systems

Accordingly to Langer [20] there are two methods to blend gases:

1. The individual components may be inserted successively into the same constant volume and the mole fractions are then calculated from the corresponding pressure increments.

2. The pressure of each component may be measured separately in a constant volume and then completely transferred to a storage chamber.

Many companies offer solutions for mixing gases through thermal mass flow controllers, such as *WitGas, Flusys.de, Testem* or *LT Gastechnick*. Its work principle is accordingly the equation 2.2:

$$\dot{Q} = \dot{m} c_p \Delta T \tag{2.2}$$

The gas will pass through a heated surface, and the amount of heat needed to supply to the surface to keep it at the same temperature is the same that was transferred into the gas. Temperature is measured before and after the resistance, which will enable obtaining the specific heat at constant pressure and the temperature difference. With the three variables known, the mass flow rate is obtained. Mass not being influenced by varying temperature or pressure is the main advantage of calculating mass flow rate [21].
Other equipment in the mixing systems companies offer are pressure regulators and shut-off valves.
Hagos, Aziz, and Sulaiman [17] tested different Syngas mixtures in an ICE. The mixture was done through flow meters, however, no detailed information was added on how it was developed. Ma, Wang, Wang, *et al.* [22] detailed how he developed a mixing system to test different mixtures of $H_2$ and $CH_4$, during engine operation. They used flow meters to measure both flows. $CH_4$ mass flow rate was kept constant and $H_2$ line had a flow controller that allowed them to vary mass flow and, consequently, change the gas mixture. Both gases would then converge in a 60 $L$ tank, to stabilize pressure oscillations and ensure the gas was mixed homogeneously.
Although mass flow controllers are the mainstream option for gas mixing, they are expensive. Furthermore, *Kolbenmaschinenlabor* wanted a simpler in-house solution to simplify the gas mixing process and fully adapt to its ICE test cell.

**Compressible Flows**

Since we are dealing with gases we can take advantage of their compressible properties. Isentropic flows refer to the flow of gases under conditions where entropy remains constant, meaning that the process is reversible and adiabatic [23]. The isentropic index, $k$, characterizes the relationship between the pressure and volume of a gas during an isentropic process. It is defined as the ratio of the specific heats at constant pressure and constant volume, $k = \frac{C_p}{C_v}$.

Considering figure 2.1 we see a compressible gas flow from 1 to 2. We can characterize the outflow mass rate through equation 2.3 [24],

$$\dot{m}_{th} = A\sqrt{2p_1\rho_1}\sqrt{\frac{k}{k-1}\left[\frac{p_1}{p_2}^{2/k} - \frac{p_1}{p_2}^{\frac{k+1}{k}}\right]} \tag{2.3}$$

The mass flow depends on:

- the exit section.
- the pressure and density downstream (at point 1).
- the isentropic index, $k$, of the gas.
- the pressure ratio between 1 and 2.

The second root in equation 2.3 only contains connections between the pressure ratio and the isentropic index. Thus, we can introduce the outflow isentropic function.

$$\Psi_s = \sqrt{\frac{k}{k-1}\left[\frac{p_2}{p_1}^{2/k} - \frac{p_2}{p_1}^{\frac{k+1}{k}}\right]} \tag{2.4}$$

And equation 2.3 becomes:

$$\dot{m}_{th} = A\sqrt{2p_1\rho_1}\Psi_s \tag{2.5}$$

The variation of $\Psi_s$ with the pressure ratio can be found in figure 2.2, for $k = 1.4$. As

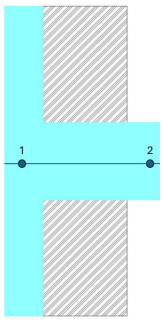



Figure 2.1: Outflow of compressible gas between 1 and 2

shown in the picture, $\Psi_s$ has function of the pressure ratio and has a parabolic shape. The

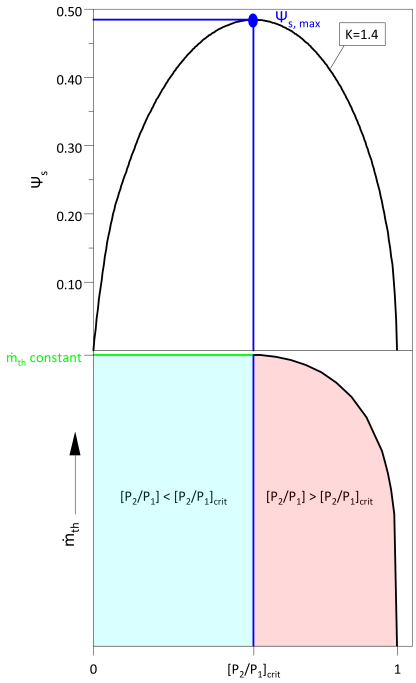



Figure 2.2: Variation of Ψ (Top) and mass flow rate (Botton) with pressure ratio.

maximum of the outflow function, $\Psi_{max}$ occurs at [24]:

$$\left[\frac{p_2}{p_1}\right]_{crit} = \left[\frac{2}{k+1}\right]^{\frac{k}{k-1}} \tag{2.6}$$

At $\Psi_{max}$ the flow exceeds the speed of sound and it becomes supersonic [23]. It was found experimentally that for flows with a lower pressure ratio than the critical one, the mass flow remains constant, regardless of the pressure downstream, $\frac{P_2}{P_1} < \left[\frac{p_2}{p_1}\right]_{crit}$ [24]. This phenomenon is referred to as *blocking* because the outlet cross-section does not allow any further increase in the mass flow by reducing the backpressure [24]. The pressure ratio at which the outlet cross-section blocks and the mass flow no longer changes is the critical pressure ratio, given by equation 2.6.

$\Psi_{max}$ is given by:

$$\Psi_{max} = \left(\frac{2}{k+1}\right)^{\frac{k}{k-1}} \sqrt{\frac{k}{k+1}} \tag{2.7}$$

Figure 2.2 shows how the mass flow changes with the pressure ratio. We can see that the mass flow remains constant for pressure ratios below the critical. In contrast, the mass flow has the same behaviour as the outflow function for pressure ratios above the critical, seen in the same figure. Table 2.10 gives some examples of critical pressure ratios for diverse gases.

To conclude, if we create a pressure differential in a compressible flow, between an exit hole, knowing the cross-section area of the exit, and maintaining the pressure ratio below

Table 2.10: Critical conditions of different gases

| Gas | $k$ | $\left(\frac{p_2}{p_1}\right)_{crit}$ | $\Psi_{max}$ |
|---|---|---|---|
| Air | 1.4 | 0.53 | 0.48 |
| Superheated steam | 1.30 | 0.53 | 0.47 |
| Saturated steam | 1.14 | 0.58 | 0.45 |
| $H_2$ | 1.41 | 0.53 | 0.48 |
| $CO_2$ | 1.29 | 0.55 | 0.47 |
| $CO$ | 1.40 | 0.53 | 0.48 |
| $CH_4$ | 1.30 | 0.55 | 0.47 |

the critical one, we will have constant and measurable mass flow through the exit. This is the principle that was used in the design of the gas mixing system, which will be better explained in chapter 3.

## Chapter 3

# Gas Mixing System Design

## 3.1 Gas Compositions and Mass Flow Rates

In chapter 1 we presented some other institutes that participate in the project. Fraunhofer-Institut UMSICHT researched and tested methods of production of Syngas obtained through different bio-residues typical from Germany such as Straw, Digestate and Sewage Sludge. To dimension the Gas Mixing System, firstly, we used reference values of biomass stocks provided by Prof. Dr. Ing. Abel Rouboua, which allowed us to start dimensioning the system. However, after the kick-off of the project, Fraunhofer-Institut UMSICHT provided us with the typical gas composition of the three feedstocks mentioned above, which we then updated in the dimensioning files. The Syngas complete compositions are shown in Appendix A in table A.1. From those values, we computed the compositions of the gases if they were only composed by $H_2$, $CH_4$, $CO_2$ and $CO$ since the other ones would be filtered out after Syngas production.

Then, to calculate the mass fraction of the gases we used the physical properties shown

Table 3.1: Syngas Volumetric Compositions Considered in Dimensioning the Gas Mixing System

| Gas | Straw | Digestate | Sewage Sludge |
|---|---|---|---|
| $H_2$ | 35.5% | 40.9% | 52.1% |
| $CO_2$ | 24.2% | 26.1% | 17.3% |
| $CO$ | 26.3% | 21.0% | 21.9% |
| $CH_4$ | 14.1% | 12.1% | 8.7% |

in table 3.2. LHV and molar mass were taken from Heywood [7]. *Gas Constant* (R) and $k$ (gas isentropic index) were taken from Coelho [25]. The notation used for mass fraction and molar fraction is the one used in Turns [11],

- mass fraction (Y),
- molar fraction ($\chi$).

Table 3.2: Gas Properties

| Gas | LHV $[kJ/kgK]$ | Molecular Weight $[g/mol]$ | R $[J/kgK]$ | $k$ at T=300 K |
|---|---|---|---|---|
| $H_2$ | 120000 | 2 | 4124 | 1.405 |
| $CO_2$ | 0 | 44 | 188.9 | 1.288 |
| $CO$ | 10132 | 28 | 296.9 | 1.4 |
| $CH_4$ | 49949 | 16 | 518.3 | 1.303 |

Then we proceeded to calculate the corresponding mass fractions of each element in the Syngas, through equation 3.1,

$$Y_{i,j} = \frac{\chi_{i,j} \times M_i}{\sum_{i=1}^{i=4} \chi_{i,j} \times M_i} \tag{3.1}$$

being,

- $i$ the element and $j$ the Syngas type.

With the mass fractions, we were able to calculate the LHV and R of each Syngas, $j$,

$$LHV_j = \sum_{i=1}^{i=4} LHV_i \times Y_{i,j} \tag{3.2a}$$

$$R_j = \sum_{i=1}^{i=4} R_i \times Y_{i,j} \tag{3.2b}$$

Subsequently, we advanced to calculating the stoichiometric air requirement of each Syngas.
To calculate the stoichiometric mass air fuel ration ($(A/F)_s$) requirement of each gas we considered equation 3.3, with air having 1 mole of $O_2$ and 3.76 moles of $N_2$ (21% of $O_2$ and 79% of $N_2$). For simplicity, the known values, the molar fractions of the elements, are represented with the notation used above and the unknowns are represented with $a$, $b$, $c$ and $d$.

$$\chi_{H_2}H_2 + \chi_{CO_2}CO_2 + \chi_{CO}CO + \chi_{CH_4}CH_4 + a\,(O_2 + 3.76N_2) \rightarrow bCO_2 + cH_2O + dN_2 \tag{3.3}$$

Taking into account that the number of each particle needs to be the same between the reactants and the products, we have the following system of equations to obtain $(A/F)_s$.

$$\text{C:} \quad \chi_{CO_2} + \chi_{CO} + \chi_{CH_4} = b \tag{3.4a}$$

$$\text{H:} \quad \chi_{H_2} + 2 \times \chi_{CH_4} = c \tag{3.4b}$$

$$\text{O:} \quad (b - \chi_{CO_2}) + \frac{(c - \chi_{CO})}{2} = a \tag{3.4c}$$

$$\text{Condition:} \quad \sum_{i=1}^{i=4} \chi_i = 1 \tag{3.4d}$$

With equations 3.4 the number of moles of air required to burn 1 mole of the gas ($a$) can be calculated.
Then we need to apply equation 3.5 to obtain $(A/F)_s$.

$$(A/F)_s = \frac{m_{air}}{m_{fuel}} = \frac{n_{air} \times M_{air}}{n_{fuel} \times M_{air}} = \frac{a\,(M_{O_2} + 3.76 \times M_{N_2})}{\sum_{i=1}^{i=4} \chi_i \times M_i} \tag{3.5}$$

To assess if the Syngas would be able to be applied into ICE we then calculated the MHV and compared those values with values from Verhelst and Wallner [2]. This property was calculated for stoichiometric conditions ($\lambda = 1$), at 300 K and pressure = 1 bar. Mixture heating value is how much energy is stored in 1 $m^3$ of the air-fuel mixture. It is calculated through equations 3.6, from Pischinger [8].

$$MHV = \frac{LHV_j \times \rho_{j+air}}{\lambda \times (A/F)_s + 1} \tag{3.6a}$$

$$\rho_{j+air} = \frac{P}{R_{j+air} \times T} \tag{3.6b}$$

$$R_{j+air} = \frac{R_j \times m_j + R_{air} \times m_{air}}{m_j + m_{air}} \tag{3.6c}$$

In tables 3.3 and 3.4 are presented all the values mentioned above. It's important to compare the values in table 3.4 with the ones in table 2.3. Syngases LHV is significant lower than the $H_2$ one. However, as can be seen by the MHV, all the gases analysed have a value similar to the fuels analysed in table 2.3. This means that even with a much lower LHV, the gases we are going to test will still be able to perform in an ICE. It happens because of the different air mass requirements each fuel has for stoichiometric combustion. Since our gases have much lower air requirements, most of the stoichiometric mixture will be composed of fuel, which increases their MHV.

Table 3.3: Mass fractions, $Y$, in %

| Element | Straw | Digestate | Sewage Sludge |
|---|---|---|---|
| $H_2$ | 3.38 | 4.07 | 6.44 |
| $CO_2$ | 50.76 | 57.08 | 47.05 |
| $CO$ | 35.10 | 29.23 | 37.9 |
| $CH_4$ | 19.75 | 9.62 | 8.6 |

Table 3.4: Calculated Properties

| Properties | Straw | Digestate | Sewage Sludge |
|---|---|---|---|
| LHV $[kJ/kg]$ | 12989.66 | 12647.25 | 15867.13 |
| R $[J/kgK]$ | 395.42 | 412.17 | 511.63 |
| $(A/F)_s$ | 3.87 | 3.76 | 4.62 |
| MHV $[MJ/m^3]$ | 3.20 | 3.14 | 3.21 |

Calculating the necessary flow rates was now possible with the mass fractions obtained. It was considered the ICE used in Wittek, Cogo, and Prante [13] since it will be used in our tests, which will be presented in further detail ahead. Its power output at full load is 100 $kW$ with an efficiency of $\eta = 35\%$. Mass flow rate of gas, $j$, $\dot{m}_j$, was calculated from fuel

conversion efficiency equation 3.7, from Heywood [7],

$$\eta = \frac{P}{LHV \times \dot{m}_j} \tag{3.7}$$

With the total mass flow of each gas, $j$, and the mass fractions, we can calculate the mass flow rate needed for each element, $i$, in each gas, as can be seen in equation 3.8 The values can be seen in table 3.5.

$$\dot{m}_i = \dot{m}_j \times Y_i \tag{3.8}$$

Table 3.5: Mass flow rates of each Syngas and element, in $kg/h$

| Element | Straw | Digestate | Sewage Sludge |
|---|---|---|---|
| $H_2$ | 2.68 | 3.31 | 4.18 |
| $CO_2$ | 40.20 | 46.42 | 30.50 |
| $CO$ | 27.8' | 23.77 | 24.57 |
| $CH_4$ | 8.52 | 7.83 | 5.58 |
| $\dot{m}_j$ | 79.1839 | 81.3277 | 64.8240 |

## 3.2 Dimensioning the Gas Mixing System

The Gas Mixing Unit contains a pressure regulator, a shut-off valve, a section with an orifice to create the isentropic outflow section, presented in chapter 2, a mixing pipe and a 100 $L$ tank to stabilize pressure oscillations and ensure the gas was mixed homogeneously. The Piping and Instrumentation Plan (P&ID) of the system is presented in Appendix B.1. The gas would leave the bottle at approximately 300 bar and the pressure would be reduced to 30 bar in a pressure regulator. To dimension the pressure regulators to each element we converted each mass flow into normalized volumetric flow (at $P = 1$ $bar$ and $T = 273.15$ $K$) through equation 3.9,

$$\dot{V}_i = \frac{\dot{m}_i \times R_i \times T}{P} \tag{3.9}$$

we considered the maximum mass flow rate for each element, between the three Syngases. The calculated values are in table 3.6. With the normalised volume flow rate, we were

Table 3.6: Normalized flow rates for each element $i$

| | $H_2$ | $CO_2$ | $CO$ | $CH_4$ |
|---|---|---|---|---|
| Max $\dot{m}_i$ $[kg/h]$ | 4.18 | 46.42 | 27.80 | 8.52 |
| $\dot{V}_i$ $[Nm^3/h]$ | 46.42 | 23.64 | 22.25 | 11.90 |

able to dimension the pressure regulators, ensuring they were capable of working with our desired flow rates.

After the pressure regulator, the gas pressure is around 30 $bar$. Then, we force the gas to

pass through an orifice, ensuring the pressure upstream of the orifice is 30 *bar*. Depending on each element's isentropic index, $k$, the mass flow rate is constant while the pressure ratio between upstream and downstream of the orifice is below the critical pressure ratio. In those conditions, the mass flow rate only depends on the section area of the orifice, the pressure and the volumetric mass upstream. To alter the composition of the gases we would change the diameter of the orifice, calculated through equations 2.5 and 2.7. When the pressure ratio equals the critical one, the electrical shutoff valves are activated, stopping the production of the Syngas. It was considered the downstream pressure as the Settling Tank pressure. When its pressure is below 12 *bar* the shutoff valves are open and the production of Syngas resumes until it reaches 15 *bar* again. We also considered a Cd of the orifice of 60%. Tables 3.7 and 3.8 show the calculated diameter of the orifices, for the three Syngases composition and the variables used.

Table 3.7: Orifices Calculation

| Variables | $H_2$ | $CO_2$ | $CO$ | $CH_4$ |
|---|---|---|---|---|
| $k_{T=300K}$ | 1.41 | 1.29 | 1.4 | 1.3 |
| $\rho_{p=30bar}$ $[kg/m^3]$ | 2.42 | 52.94 | 33.68 | 19.29 |
| $\Psi$ | 0.48 | 0.47 | 0.48 | 0.47 |
| $P_2/P_1$ | 0.53 | 0.55 | 0.53 | 0.55 |
| $P_2$ limits $[bar]$ | 15.82 | 16.44 | 15.85 | 16.36 |

Table 3.8: Orifices diameter in [mm]

| Diameter [mm] | $H_2$ | $CO_2$ | $CO$ | $CH_4$ |
|---|---|---|---|---|
| Straw | 0.93 | 1.68 | 1.54 | 0.99 |
| Digestate | 1.02170 | 1.8074 | 1.43 | 0.95 |
| Sludge | 1.15 | 1.47 | 1.45 | 0.80 |

The automated shut-off valves aim to allow using the gas mixing system while ICE operation, at various loads. In figure 3.1 we can see how much time it takes for the unit to fill the tank from 10 to 15 *bar*. This was calculated from equations 3.10 and allows us to have an estimate of how many times the shut-off valves will work during ICE operation. However, it also depends on the load at which the engine is running, because in the worst-case scenario, the mixture produced will be the same as the mass flow requirements of the engine at full load. Equations 3.10 allowed us to see how much time each gas fills the 100

$L$ tank from 10 $bar$ to 15 $bar$.

$$t = \frac{\Delta m}{\dot{m}} \tag{3.10a}$$

$$t = \frac{m_{15bar} - m_{10bar}}{\dot{m}} \tag{3.10b}$$

$$t = \frac{\rho_{15bar} \times V_{100L} - \rho_{10bar} \times V_{100L}}{\dot{m}} \tag{3.10c}$$

$$t = \frac{\frac{P_{15bar}}{RT} \times V_{100L} - \frac{P_{10bar}}{RT} \times V_{100L}}{\dot{m}} \tag{3.10d}$$

$$t = \frac{(P_{15bar} - P_{10bar}) \times V_{100L}}{RT \times \dot{m}} \tag{3.10e}$$

$$\tag{3.10f}$$

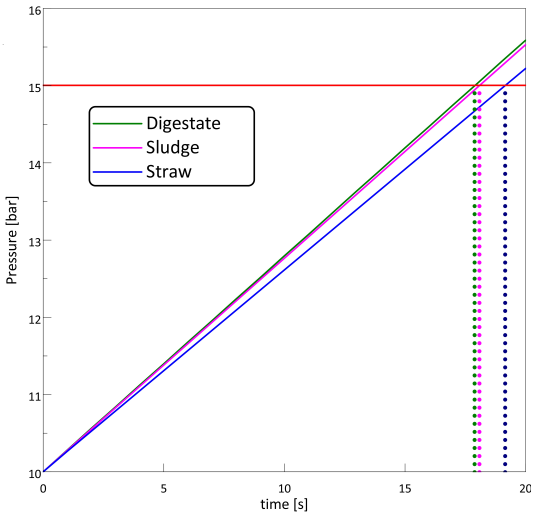



Figure 3.1: Time to fill the 100 $L$ tank from 10 $bar$ to 15 $bar$.

From figure 3.1 we see that the Syngas made from Straw requires the most time since it has the lowest denominator, $RT \times \dot{m}$.

## 3.3 Defining the Parts

We needed to dimension the parts in the P&ID plan in figure B.1 to ensure a reliable mixing unit. Those are the following:

- Pressure Regulators,
- Shut-off valves,
- Mixing Pipe,
- Orifices.

The mixing unit would be applied directly into the existing $H_2$ supply line of the $H_2$ ICE test cell. Consequently, the mixing unit piping has the same size as the $H_2$ supply line, which is 12 *mm* .
The settling tank comprises two old $CO_2$ 50$L$ tanks.

**Pressure Regulator**
When choosing the adequate pressure regulator we had to take into account the following factors:

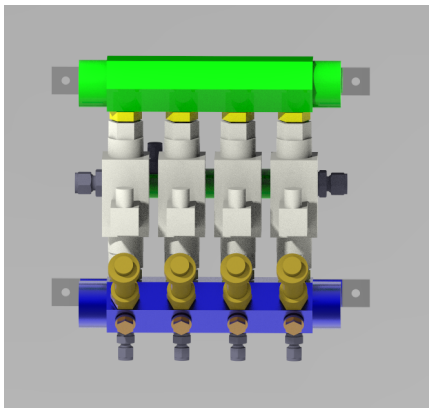
- Material, we need to ensure that the gas component will not damage the pressure regulator,
- Flow Coefficient (Cv), important to guarantee that the desired flow rate will pass through the regulator at the desired pressure,
- Pressure, select a pressure regulator that can work in the desired pressure range.

After some research, it was found that few companies offered solutions for pressure reducers from 300 to 30 *bar*. We chose WK-ARMATUREN [26] pressure-reducing station for Oxygen and non-corrosive gases with a safety pressure gauge to limit the pressure in the pressure regulator to 75 *bar* and fittings for the inlet and outlet. Its specifications can be seen in Appendix C.

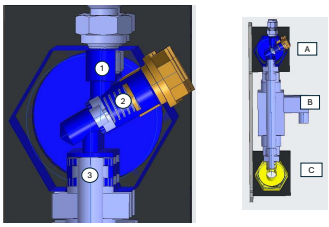
**Shut-off Valves**
As for the shut-off valves we had to ensure that the gas component would not damage it, furthermore, we had to focus, on quick actuation times, to ensure good accuracy and actuation mechanisms. Finally, we focused on the Cv, which describes the pressure loss through an orifice. We wanted to be sure that the shut-off valve would have a low influence on the fluids pressure, that's why we've placed them after the orifice, not to affect the flow rate.
The valve chosen was an axial shut-off valve with electrical actuation from Co-Ax [27], mainly because of its rapid actuation time (25 *ms*). Its specifications can be seen in Appendix C.

**Orifice and Mixing Pipe**
These components were designed by Prof. Witteck and produced in *Kolben Maschinen Labor*. A single component receives the 4 gas components through independent designated channels. Each channel has 4 ports, a gas inlet, a gas outlet, a port to connect a pressure measurement device upstream of the orifice, and one port to connect the orifices for each gas. It's represented in figure 3.2b. Each outlet is connected to the designated shut-off valve. The mixing pipe is connected to all 4 shut-off valve outlets. It can be seen in figures 3.2a and 3.2b. Hole number 1 is the gas inlet, number 2 is the housing for the orifice and number 3 is the gas outlet. The channel for the pressure measurement device is not

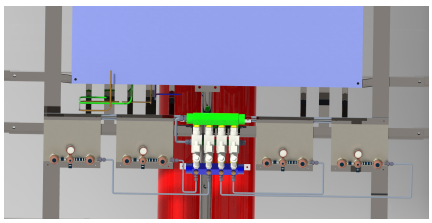
represented. Component A receives the 4 gases independently, houses the orifices and its outlet is connected to the shut-off valve, component B, whose outlets are connected to component C, where all 4 gases mix. Figure 3.2c shows the 3D model of the mentioned components connected to the $H_2$ supply line.



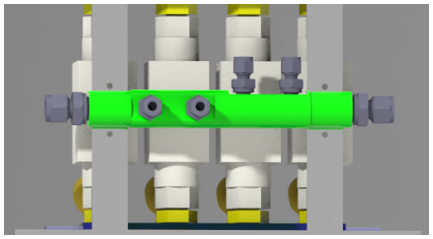
(a) 3D model of the Mixing Panel.




(b) 3D model of Component A that houses the orifices and the Mixing Pipe, C. Component B is the shut-off valves.



(c) 3D model of the Gas Mixing Unit connected to the existent $H_2$ supply line.



(d) 3D model of the Flute that diverts the flow to both bottles and connects each bottle's outlet flow.

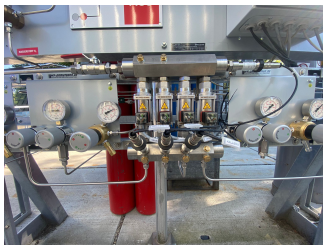
Figure 3.2: Various 3D models of the Gas Mixing System components.

To conclude the dimensioning, we also had to choose adequate fittings to connect these components to each 50 $L$ bottle and the piping. For the first case, Prof. Wittek designed a flute that would receive, in one end, the flow from the mixing pipe and divide that flow to each bottle. Then the flute would connect the outlet flow from each bottle and its outlet is connected to the supply line of the test cell. The flute 3D CAD can be seen in figure 3.2d. The main focus for the remaining fittings was that they would have the same diameter as the existing piping, 12 *mm*, and good sealing to ensure no gas losses. The fitting chosen were:

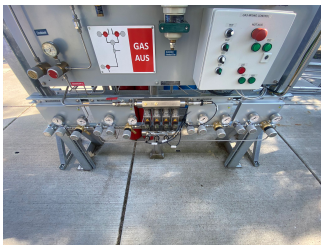
- Connection between the Pressure Regulator and the pipping,
- Connection of the piping to each channel in component A from figure **??**,
- Connection between the mixing pipe and the piping,
- Diversion of the piping to each 50 $L$ settling tank,
- Conversion of each settling tank outlet to the piping,

- 3 way ball valve to connect the Syngas line to the existing supply line,
- Fittings for the inlet and outlet of the shut-off valves, designed by Prof. Witteck and produced at *Hochschule Heilbronn*.

We chose fittings with a straight shoulder to place a sealing, O-Ring, to minimize gas leakage.
In figure 3.3 it can be seen how these components were mounted in the existent infrastructure of the test cell. In figure 3.3c can be seen that only a 50 $L$ bottle is connected, since it was the trial phase of the system and we wanted to ensure that no gas would be wasted.



(a) Mixing Panel.




(b) Gas Mixing Unit.



(c) Flute.

Figure 3.3: Gax Mixing Unit components mounted in the existent infrastructure.

## 3.4 Gas Characterization

Several values characterizing the Syngases to be tested have already been presented. Those properties can be seen in table 3.4. However, for a better knowledge of the gases, there are some properties to be known:

- Laminar flame speed,
- Adiabatic flame temperature,
- Lower flammability limit,
- Upper flammability limit,
- Minimum ignition energy.

**Laminar flame speed**
We tried to compute laminar flame speed through a Cantera [28] open-source code. However, as stated in chapter 2, it's difficult to measure and compute LFS of high $H_2$ content

Syngas at high pressure with reasonable accuracy because of discrepancies between modelled and experimental data. Although we were able to compute plausible results for $H_2$, the results obtained for $CH_4$ and $CO$ were very far from experimental ones which led us to dismiss the computed values for the Syngases.
The open-source code used can be seen in appendix D.

**Adiabatic flame temperature**

Through a Cantera open-source code, we computed the adiabatic flame temperature along different *A/F* ratios. We compared the values obtained for $H_2$ and $CH_4$ with values in Heywood [7] and got similar results. In figure 3.4 we compare the computed adiabatic flame temperatures along different $\lambda$ of $H_2$ with the computed for Syngases. Appendix D shows the open-source code used to calculate these values.

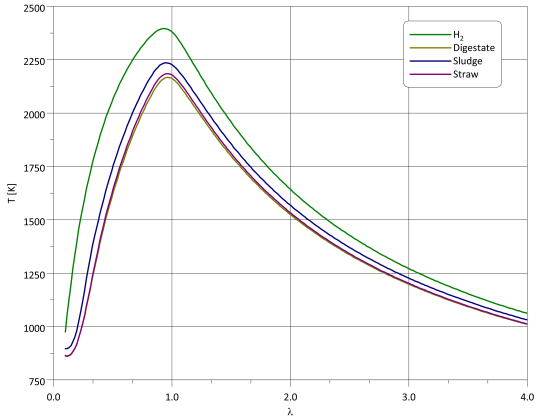



Figure 3.4: Computed adiabatic flame temperature for $H_2$ and the three Syngases.

**Minimum Ignition Energy**

With the above values, it would be possible to calculate the MIE, through equation 2.1. The physical properties were obtained through *EES* software, which can also be seen in appendix D. However, since the LFS results were inaccurate it resulted in MIE values that didn't correspond to the ones in the literature. This property is important to characterize the flammability limits of the Syngases, which is the $\lambda$ which correspondent MIE is not feasible to deliver to the fuel+air mixture. In figure 3.5 can be seen a plotted graph with the calculated values of MIE for $H_2$, varying $\lambda$, which is the relation between the $(A/F)$ of the mixture with the stoichiometric $(A/F)$.

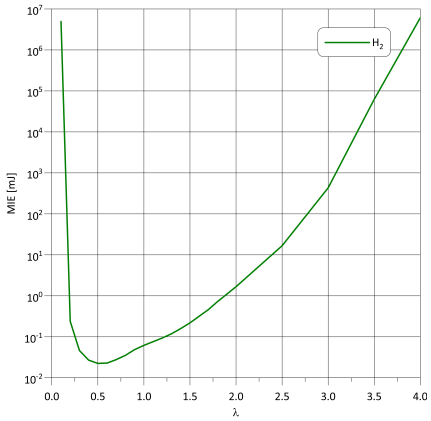



Figure 3.5: Computed MIE for $H_2$.

**Lower Flammability Limit**

Since the computed MIE were not accurate we computed the LFL through *Le Chatelier's* formula [29]. However, it is not possible to calculate the upper flammability limit through this technique. *Le Chatelier's* consist of equations 3.11, 3.12 and 3.13. Equation 3.12 is an adjustment to the LFL since our gas mixture contains an inert gas, $CO_2$.

$$LFL_M = \frac{100}{\sum_i^n \frac{A_i}{LFL_i'}} \tag{3.11}$$

$$LFL_i' = \frac{\left(100 - LFL_M' - (1-\overline{K})\frac{\sum_{p=1}^{k} B_k}{\sum_{i=1}^{n} A_i} \times LFL_M'\right)}{(100 - LFL_M')} \times LFL_i \tag{3.12}$$

$$LFL_M' = \frac{100}{\sum_i^n \frac{A_i}{LFL_i}} \tag{3.13}$$

$LFL_M'$ is the lower flammability limit of the mixture of only flammable gases. $\overline{K}$ is the nitrogen equivalency of the inert gases. $A_i$ is the molar fraction based of the flammable gases, $i$, of the gas mixture. $B_k$ is the molar fraction of the inert gas, $k$, of the gas mixture. We considered the following LFL and $\overline{K}_{CO_2}$ values in the calculation, from [29]:

- $LFL_{H_2} = 4$
- $LFL_{CH_4} = 4$
- $LFL_{CO} = 12.5$
- $\overline{K}_{CO_2} = 1.5$

The results obtained are in table 3.9.

Table 3.9: LFL calculations in %mol

| | Straw | Digestate | Sludge |
|---|---|---|---|
| $LFL'_M$ | 6.89 | 6.7 | 5.46 |
| $LFL'_{H_2}$ | 4.05 | 4.05 | 4.02 |
| $LFL'_{CH_4}$ | 12.65 | 12.66 | 12.57 |
| $LFL'_{CO}$ | 4.05 | 4.05 | 4.02 |
| $LFL_M$ | 6.98 | 6.78 | 5.49 |
| $\lambda'$ | 23.27 | 25.65 | 30.48 |

We then established a relationship between the LFL $H_2$ value in Schröder [29] and the operating LFL in $H_2$ ICE operation in Wittek, Cogo, and Prante [13] tests. It was possible to obtain the LFL $\lambda$ for engine operation, which can be seen in table 3.10.

Table 3.10: $\lambda$ values for ICE operation.

| | $H_2$ | Straw | Digestate | Sludge |
|---|---|---|---|---|
| $\lambda'$ | 48.03 | 23.27 | 25.65 | 30.48 |
| $\lambda$ | 4 | 1.94 | 2.14 | 2.54 |

## Chapter 4

# Experimental Investigation

## 4.1 Internal Combustion Engine and Measurement Devices

This chapter will discuss the tests made with the Syngas, produced in the gas mixing unit, in an ICE. First, we will characterize the ICE and the measurement devices. It was used the same setup as in Wittek, Cogo, and Prante [13]. Then, we will present the tests that were made, to evaluate the accuracy of the gas mixing system and how Syngas compares with $H_2$ in an ICE.

The engine used in the tests was a series diesel 'TCD 3.6' from *Deutz*, converted for $H_2$. It is a 4-cylinder inline, four-stroke, water-cooled, DI diesel engine with turbocharging. Its technical data can be seen in table 4.1.

Table 4.1: Technical data of the series 'TCD 3.6' from *Deutz*

| | |
|---|---|
| Cylinder Bore ($\phi$) | 98 [$mm$] |
| Piston Stroke | 120 [$mm$] |
| Displacement | 3621 [$cm^3$] |
| Connecting Rod Length | 184.5[$mm$] |
| Compression Ratio | 17.2 |
| Max. power at speed | 100 [$kW$] at 2000 [$mm^{-1}$] |
| Max. torque at speed | 500 [$Nm$] at 1600 [$mm^{-1}$] |
| Exhaust valve lift, duration and max. position | 8.87 [$mm$], 268 [$dCA$], 98 [$dCA\ BTDC$] |
| Intake valve lift, duration and max. position | 8.88 [$mm$], 257 [$dCA$], 98 [$dCA\ ATDC$] |

The ICE was then converted to $H_2$ operation at *Kolben Maschinen Labor*. It included the following measures:

- Reduction of the geometrical compression ratio,
- Application of an ignition system,
- Application of a gas injection system.

The geometrical CR was reduced to 10 and a rotationally symmetrical bowl was incorporated.

An ignition system was applied that comprised one spark plug and one ignition coil per cylinder. Spark plug mounting holes were drilled as close as possible to the cylinder axis. The spark plug used is a cold-rated spark plug for motorsport applications. The ignition coil used is a prototype ignition coil.

The mixture formation method selected was PFI. The fuel gas is metered cyclically by electromagnetically actuated injectors. Two injectors are connected via an injector adapter to meet the required flow capacity to form one unit per cylinder. The fuel gas is supplied to the injectors via an $H_2$ fuel rail. The fuel injectors used are commercially available PFI injectors, originally designed for gaseous fuels such as CNG or Liquified petroleum gas (LPG).

**Measurement Devices**

The ICE was installed in the $H_2$ engines test facilities of the *Kolben Maschinen Labor* of the University of Applied Sciences of Heilbronn. It was coupled to an eddy current brake, allowing operation at constant speed conditions. The brake torque was measured with a torque flange (HBM, type T40, $1kNm$). The absolute pressure in the hydrogen fuel rail was regulated to a constant 6 bar by a mechanical pressure regulator.

An indicating system was used for combustion analysis, allowing crack angle synchronous data acquisition (Kistler, model Kibox, 1st generation). A crank angle encoder was installed in the engine's crankshaft pulley (Kistler, type 2614C11). The instantaneous crank position can be known with a $0.1^\circ$ resolution.

In-cylinder pressure was measured at each cylinder with water-cooled piezoelectric pressure transducers (Kistler, type 6041A) while the pressure signals passed through amplifiers (Kistler, type 5064B).

All signals other than the in-line cylinder and the in-port pressures were recorded using a time-based low-frequency data acquisition system. The absolute pressure measurement was performed with Keller type PAA-33X transducers (0.8-1.2 bar upstream compressor, 0-100 *bar* fuel supply pressure, 0-10 *bar* at all other places) while relative pressures were obtained with Keller type PR-33X transducers (0-10 *bar*). Temperatures were acquired with type-K thermocouples. The intake air mass-flow rate was measured with an air mass flow sensor (ABB, type Sensyflow FMT700-P, 0-1200 $kg/h$), mounted downstream of the air filter. The fuel mass-flow rate was measured with a Coriolis mass-flow meter (Endress+Hauser, type Promass A300, 0-33 $kg/h$ of $H_2$). A gas analyser (Ecophysics, type CLD700, 0-10000 $ppm$ of $NO$ and $NO_x$) was mounted downstream of the turbine to obtain the $NO_x$ raw emissions. Finally, a Syngas composition analyser was acquired (*MRU VARIOluxx*), which was coupled to the fuel rail bar, allowing us to be fully certain of how the gas composition varies throughout the tests.

A schematic of the Gas Mixing System and of the ICE its measurement points can be seen in figure E.1. Figure E.2 shows the ICE mounted in the $H_2$ test cell.

A series of 4 different tests were made:

1. Calculation of Cd of the orifices,
2. Analysis of the Gas Measurement System and evaluation of the behaviour of the Gas Mixing System,
3. Load-cut at 1500 *RPM* with 100% $H_2$,
4. Load-cut at 1500 *RPM* with 90% $H_2$ and 10% $CO_2$.

## 4.2 Calculation of Cd of the orifices

To test the Gas Mixing System with application in the ICE we decided to test a composition of 75% $H_2$ and 25% $CO_2$. As explained in sections 3 and 2.2, with equation 3.7 it was calculated the total mass flow required for the Syngas composition. With equation 3.8 we obtained the theoretical mass flow required of each gas ($H_2$ and $CO_2$) to create the desired mixture. With equations 2.4 and 2.7 we achieved the orifice diameter. The data used is the same as in table 2.10 and is resumed in table 4.3 Then, for each of the orifices, we used $N_2$.

Table 4.2: Theoretical orifices diameter calculation for 30 *bar* and 300 *K* upstream of the nozzle.

| | $H_2$ | $CO_2$ |
|---|---|---|
| $Cd_{th}$ | 60% | 60 % |
| $R_i$ $[J/kg\dot{K}]$ | 4124 | 188.9 |
| $\rho$ $[kg/m^3]$ | 2.42 | 52.94 |
| $k_{T=300K}$ | 1.41 | 1.29 |
| $\Psi_{max}$ | 0.48 | 0.47 |
| $\dot{m}_{th}$ $[kg/h]$ | 8.02 | 56.85 |
| Diameter $[mm]$ | 1.6 | 2 |

We redid the calculations to see how much flow would be expected of each orifice but with $N_2$. Then, we tested the orifice, measuring the pressure and temperature upstream of the nozzle and the mass flow. For accuracy, each orifice was tested several times. The results are shown in table 4.3 These tests were made with a particular device manufactured for that

Table 4.3: Cd calculation for the orifice with 1.6 mm and 2 mm diameter.

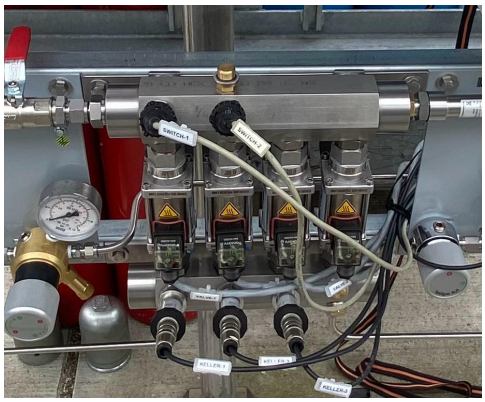
| d=1.6 $[mm]$ | $P_{avg}$ $[bar]$ | $T_{avg}$ $[K]$ | $\rho_{avg}$ $[kg/m^3]$ | $\dot{m}_{th}$ $[kg/h]$ | $\dot{m}_{avg}$ $[kg/h]$ | Cd |
|---|---|---|---|---|---|---|
| Test 1 | 25.37 | 26.14 | 28.56 | 42.15 | 38.36 | 0.91 |
| Test 2 | 21.43 | 27.08 | 24.05 | 42.15 | 35.55 | 0.90 |
| Test 3 | 26.40 | 26.85 | 29.65 | 43.82 | 39.78 | 0.91 |
| Test 4 | 33.29 | 26.66 | 37.41 | 55.28 | 50.32 | 0.91 |
| d=2 $[mm]$ | | | | | | |
| Test 5 | 21.72 | 25.93 | 24.46 | 56.41 | 52.51 | 0.93 |
| Test 6 | 23.90 | 26.13 | 26.91 | 62.06 | 57.28 | 0.92 |
| Test 7 | 26.35 | 26.13 | 29.66 | 68.41 | 64.14 | 0.94 |

purpose (figure E.3), where downstream the nozzle was at ambient pressure. The pressure fluctuations between tests were because of difficulties with regulating the pressure regulator since when the shut-off valve opened, pressure would decrease. However, it did not impact the test results, since we measured and considered the other variables that influence the mass flow through the orifice.

Since both orifices have similar Cd's, the real composition is not significantly altered (a difference of 0.2% in terms of molar composition, and 0.4% in terms of mass composition).

## 4.3 Analysis of the Gas Measurement System

This series of tests is intended to evaluate the behaviour of the Gas Mixing System. First, we examined whether altering the gas selection input in the Coriolis Mass Flow Meter would affect the mass flow value output, but found no change.
Then, we evaluated the behaviour of the Gas Mixing System. We found a problem with the pressure switches that control the shut-off valves to close when the pressure downstream the orifices is above 15 *bar* and to open when the pressure is below 12 *bar*. It was found a malfunction with the switches that made the shut-off valves work in a loop because the switches were placed right after the orifices exit. This happened because of high pressure upstream of the orifices when the shut-off valves were closed. When the pressure would be below 12 *bar* and the shut-off valves opened upstream, the switches would be activated to close the valves because of localized high pressure points. Then, the switch would be deactivated because the pressure downstream the orifices would not rise above 12 *bar*. To correct this problem, the switches were placed after the settling tank. This way, we could benefit from the high volume of the tank to reduce pressure waves and ensure a good function of the system. In figure 4.1 we can see the initial setup and the final one.



(a) Old configuration of the pressure switches.



(b) New configuration of the new pressure switches.

Figure 4.1: Old and new configurations of the pressure switches

Lastly, we tested the composition produced by the Gas Mixing System. A Syngas composition analyser from *MRU* was coupled to the fuel rail bar allowing us to see how the composition behaved while the ICE was running. We intended:

- Composition of 90% $H_2$ and 10% $CO_2$,
- Shut-off valves to open when the pressure downstream the orifices was 12 *bar* and to close at 15 *bar*,
- Pressure upstream the orifices of 30 *bar*.

At the bottom of figure 4.2 we can see the behaviour of the shut-off valves. If we compare with the pressure downstream we can see that the shut-off valves open and close at approximately 12 and 15 *bar*, respectively. We can see the pressure downstream above and below the stipulated pressure because of the time it takes for the signal to be delivered to the valves and for them to close. This does not jeopardize the gas composition.
Analysing the pressure upstream of the $H_2$ and $CO_2$ orifices we see that the pressure regulators cannot maintain the upstream pressure around the 30 *bar* goal. Furthermore, figure 4.3 a) shows that the system cannot keep a constant composition. Since the $H_2$ pressure regulator showed high vibrations while operating, we believe it jeopardised the mixture composition. To fix that, we reduce the $H_2$ nozzle to limit the mass flow and, thus, reduce the vibrations. The new composition of orifices was 1.3 *mm* to $H_2$ and and 1 *mm* to $CO_2$, theoretically producing a mixture of 90% $H_2$ and 10% $CO_2$. Furthermore, we also reduced the pressure upstream of the $H_2$ pressure regulator. Figure 4.3 compares the concentration with a theoretical mixture formation of 75% $H_2$ and 25% $CO_2$ (figure a)) with a mixture of 90% $H_2$ and 10% $CO_2$ (figure b)). Reducing the pressure upstream of the $H_2$ pressure regulator and limiting the $H_2$ mass flow through a reduction of the orifice diameter allowed to maintain a constant concentration through ICE operation.
Through figure b) from figure 4.3 it can be seen that the concentration keeps constant at 83% $H_2$ and 17% $CO_2$, instead the desired 90% and 10%, respectively. This may happen because of 2 reasons:

1. No consideration of the $H_2$ heating effect in the pressure regulator and, also, the cooling effect of the $CO_2$ in the pressure regulator. This reduces $H_2$ and increases $CO_2$ density,
2. Possible leakage in the $CO_2$ orifice. If the orifice centre is not aligned with the spring centre in their housing, it may lead to the orifice not being fully seated with the exit of component A, from figure 3.2, and to $CO_2$ to leak to the exit.

Figure 4.4 shows the behaviour of the $H_2$ pressure regulator with an orifice of 1.3 *mm* thus reducing $H_2$ mass flow. It shows that limiting the pressure upstream of the $H_2$ pressure regulator and reducing the mass flow through the orifice helped to maintain the mixing pressure upstream of the orifice much closer to the design pressure of 30 *bar*.

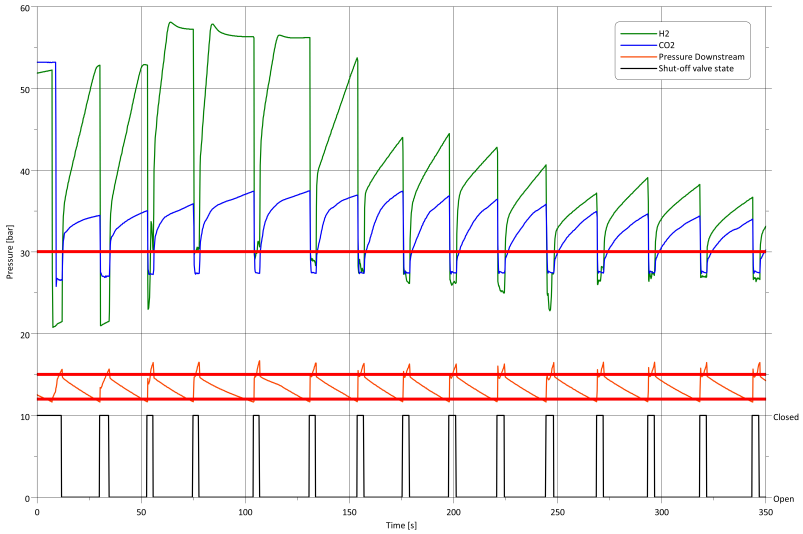



Figure 4.2: Behaviour of the Gas Mixing System.

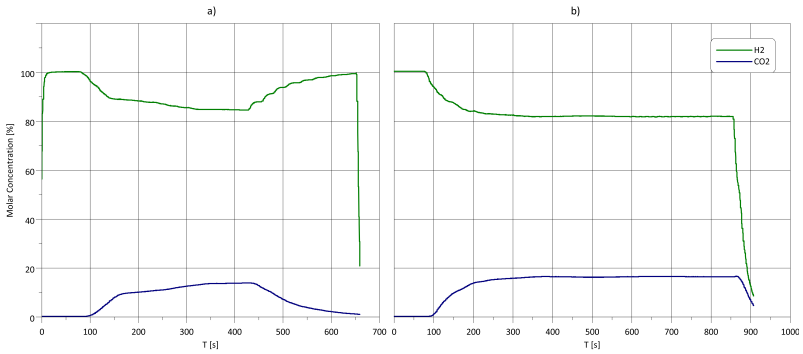



Figure 4.3: Concentrations variations. Figure a): 75% and 25%, $H_2$ and $CO_2$, respectively. Figure b): 90% and 10%, $H_2$ and $CO_2$, respectively.

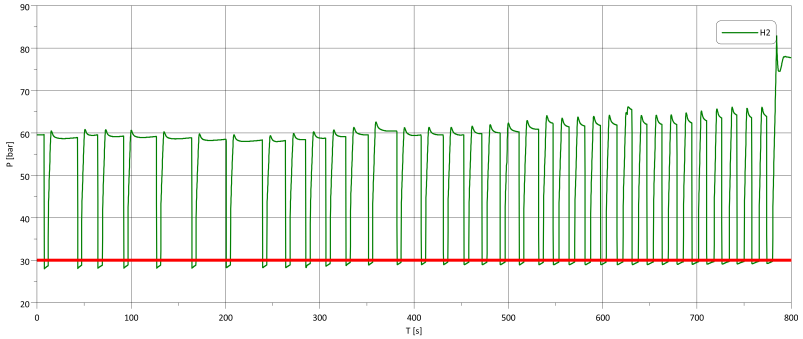



Figure 4.4: Behaviour of $H_2$ regulator with an orifice of 1.3 $mm$.

## 4.4 Comparison between 100% $H_2$ and a mixture of $H_2$ and $CO_2$

In this section, we compare the operation of 100% $H_2$ with a mixture of 83% $H_2$ and 17% $CO_2$, at 1500 $rpm$. The orifices' diameters were 1.3 $mm$ for $H_2$ and 1 $mm$ for $CO_2$ and theoretically should have produced a mixture of 90% $H_2$ and 10% $CO_2$ but, instead, due to

the reasons stated before, produced a mixture of 83% $H_2$ and 10% $CO_2$.
Blending $CO_2$ with hydrogen means we are diluting the combustible gas ($H_2$) with an inert gas ($CO_2$). We should expect a decrease in the $ISNO_x$ emissions with the gas mixture, since diluting $H_2$ will decrease the combustion temperature, which is one of the main variables in $NO_x$ formation. Furthermore, we also expect less lean combustion with the gas mixture because the inert gas reduces oxygen availability.

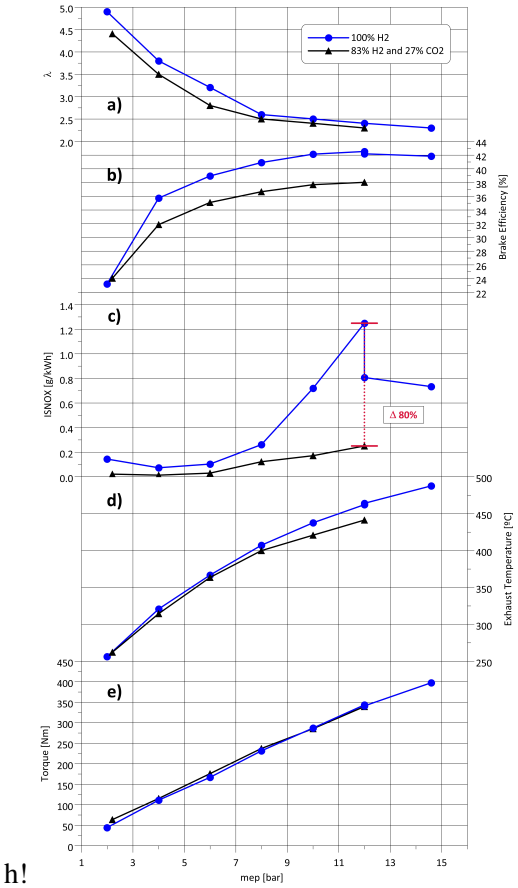
Table 4.4: Operation parameters with 100 % $H_2$

| *mep* | Spark Advance [ms] | Injection Pulse Width [$deg\ bTDC$] | $\dot{m}_{Gas}$ [$kg/h$] | $\dot{m}_{air}$ [$kg/h$] |
|---|---|---|---|---|
| 2 | 27 | 3.5 | 1.13 | 1.13 |
| 4 | 21 | 4.5 | 1.67 | 204.28 |
| 6 | 16 | 5.4 | 2.21 | 223.42 |
| 8 | 12.5 | 6.6 | 2.89 | 245.69 |
| 10 | 10.5 | 2.7 | 3.46 | 276.63 |
| 12 | 9 | 8.9 | 4.10 | 309.89 |
| 12 | 8 | 9 | 4.11 | 315.82 |
| 14.6 | 8.5 | 10.6 | 4.83 | 364.92 |

Table 4.5: Operation parameters with 83 % $H_2$ and 17 % $CO_2$

| *mep* | Spark Advance [ms] | Injection Pulse Width [$deg\ bTDC$] | $\dot{m}_{Gas}$ [$kg/h$] | $\dot{m}_{air}$ [$kg/h$] |
|---|---|---|---|---|
| 2.2 | 27 | 6.9 | 6.76 | 191.43 |
| 4 | 22 | 9 | 9.19 | 203.76 |
| 6 | 17.5 | 12.5 | 12.58 | 227.5 |
| 8 | 15 | 13.8 | 16.42 | 258.83 |
| 10 | 13.5 | 16.9 | 19.37 | 290.59 |
| 12 | 12 | 21.5 | 22.70 | 328.46 |

The test performed was a load cut at 1500 $rpm$. We evaluate the engine's response and performance at different loads with constant speed while only altering spark timing to obtain maximum brake torque. While following this strategy, at the load of 12 *bar*, the 100 % $H_2$ surpassed the 1 $g/kWh$ $ISNO_x$ emission limit defined in Wittek, Cogo, and Prante [13]. The spark timing was altered at 12 and 14 *bar* load to fulfil the emissions requirement for 100 % $H_2$ test.
In tables 4.4 and 4.5 we can compare the difference between the operation parameters of the two gases. Since the second has more energetic content, we can see that combustion is more advanced in the gas mixture than the pure $H_2$. Furthermore, the gas mixture needs a longer injection width because of the higher mass flows. Finally, as expected, the gas mixture needs more air than pure $H_2$ because the $CO_2$ reduces oxygen availability. Figure 4.5 compares some performance parameters between the two gases defined before. The first graph (graph a.) compares the $A/F$ ratio between the two mixtures at different loads. As expected, both operate with a lean mixture, as stated in [2] and the $A/F$ ratio of the $H_2$ and $CO_2$ blend is slightly richer (lower $\lambda$) because the mixture is more diluted with an




h!

Figure 4.5: ICE performance comparison between 100% $H_2$ and 83% $H_2$ + 17% $CO_2$.

inert gas and it reduces $O_2$ availability. In terms of $NO_x$ emissions, we see that the $H_2$ and $CO_2$ mixture produces lower $ISNO_x$ emissions. This is because diluting the combustible gas reduces combustion temperature, demonstrated in the Exhaust Gas temperature graph (graph c.), which is a very important variable in $NO_x$ formation. At the load of 12 *bar Mean Effective Pressure* (MEP), MBT surpassed the limit of 1 $g/kWh$ $ISNO_x$ emissions. If we compare those emissions with the $H_2$ and $CO_2$ blend ones, we see that the gas blend achieved a reduction of 80%, while maintaining a similar torque. In terms of Torque (graph e.), we can see that the $H_2$ and $CO_2$ mixture produces slightly higher torque at low loads (until 10 *bar*). Above that mark, the 100% $H_2$ produces higher torque. This happens because at low loads the presence of an inert gas helps stabilize the lean combustion process, which translates into a higher output. Furthermore, this test campaign did not test higher loads, in which the 100% $H_2$ torque would be expected to be higher than the gas mixture. To conclude the analysis of this figure, we can see that the gas mixture ass less brake thermal efficiency (graph b.), because of higher pumping losses since it requires more air per cycle, as can be seen in tables 4.4 and 4.5.

# Chapter 5

# Conclusion

The present study successfully developed and validated a gas mixing system designed to facilitate the testing of $H_2$ and Syngas mixtures in ICEs.

Throughout the research, the methodology adopted involved the careful calculation of mass flow rates for each gas component based on pressure differentials, using the principles of compressible flow. The gas mixing system was designed with an understanding of the critical pressure ratio, ensuring that the flow remained stable and measurable. The experimental tests conducted provided valuable insights into the behaviour of the system and compared a mixture of $H_2$ plus $CO_2$ with pure $H_2$ in an ICE. In the future, for more accurate mixing results, carburettor orifices will be used, since they allow an increment of 0.05 *mm*, instead of 0.1 *mm* increment we had for this tests.

The initial tests aimed at determining the Cd of the orifices were successful, establishing a reliable baseline for future evaluations. Subsequent performance tests with mixtures of $H_2$ and carbon dioxide demonstrated a reduction in $ISNO_x$ emissions, affirming the hypothesis that diluting $H_2$ with an inert gas can lead to lower combustion temperatures and, consequently, reduced emissions. This is particularly significant given the increasing regulatory pressures regarding emissions from ICEs, highlighting a potential pathway for utilizing Syngas as a cleaner alternative fuel source.

Notably, the performance tests revealed that while the $H_2$ and $CO_2$ mixture produced a lower torque at higher loads compared to 100% $H_2$, it showed improved stability and efficiency at lower loads. This finding underscores the importance of further optimizing the gas mixing proportions to enhance engine performance across different operational regimes. The experimental results indicated an 80% reduction in NOx emissions when using the gas

mixture compared to pure $H_2$, presenting a compelling case for further research into Syngas as a viable alternative fuel for ICEs.

The findings of this research lay a solid foundation for future work in several key areas:

1. Optimization of Gas Mixing Ratios: Future studies should focus on fine-tuning the proportions of $H_2$, $CO_2$, $CO$, and $CH_4$ in the Syngas mixture. This could involve extensive experimental campaigns to evaluate a wider range of Syngas compositions and their specific impacts on combustion efficiency and emissions profiles.

2. Long-term Durability Testing: Understanding the long-term effects of using Syngas in ICEs is crucial. Future research should investigate engine components' durability and wear characteristics when subjected to various gas mixtures over extended periods. This will help assess Syngas feasibility as a sustainable fuel option.

3. Integration with Advanced Engine Technologies: Exploring the compatibility of Syngas with advanced engine technologies, such as variable geometry turbocharging and direct injection systems, could yield insights into enhancing performance and efficiency. Research into hybrid systems that combine Syngas with other fuels may also be beneficial.

4. Combustion Characteristics Analysis: A detailed investigation into the combustion characteristics of Syngas mixtures, including laminar flame speed, ignition delay, and flame stability, will provide a deeper understanding of the combustion processes involved. Utilizing advanced simulation tools alongside experimental data can enhance the accuracy of these characterizations.

In conclusion, while this study has provided significant insights into the development and application of a gas mixing system for ICEs, the journey towards fully integrating Syngas as a mainstream fuel requires ongoing research and collaboration across multiple disciplines. Moreover, a key factor may be the $CO_2$ produced from the gasification processes, since biomass is a $CO_2$ retainer a strategy is needed to handle the output of this gas to not increase $CO_2$ emissions with the production of Syngas. The findings not only contribute to the current body of knowledge but also pave the way for innovative approaches to fuel utilization in the context of sustainable energy solutions.

# Bibliography


[1] E. Union. "Eu hydrogen strategy." Accessed: 2024-06-03. (2022), [Online]. Available: https://energy.ec.europa.eu/topics/energy-systems-integration/hydrogen_en.

[2] S. Verhelst and T. Wallner, "Hydrogen-fueled internal combustion engines," *Progress in Energy and Combustion Science*, vol. 35, no. 6, pp. 490–527, Dec. 2009, ISSN: 0360-1285. DOI: 10.1016/j.pecs.2009.08.001.

[3] A. H. Martins, A. Rouboa, and E. Monteiro, "On the green hydrogen production through gasification processes: A techno-economic approach," *Journal of Cleaner Production*, vol. 383, p. 135 476, Jan. 2023, ISSN: 0959-6526. DOI: 10.1016/j.jclepro.2022.135476. [Online]. Available: https://www.sciencedirect.com/science/article/pii/S0959652622050508 (visited on 05/31/2024).

[4] S. R. Naqvi, B. kazmi, S. A. Ammar Taqvi, W.-H. Chen, and D. Juchelková, "Techno economic analysis for advanced methods of green hydrogen production," *Current Opinion in Green and Sustainable Chemistry*, p. 100 939, May 2024, ISSN: 2452-2236. DOI: 10.1016/j.cogsc.2024.100939. [Online]. Available: https://www.sciencedirect.com/science/article/pii/S2452223624000609 (visited on 05/31/2024).

[5] M. A. Habib, G. A. Q. Abdulrahman, A. B. S. Alquaity, and N. A. A. Qasem, "Hydrogen combustion, production, and applications: A review," *Alexandria Engineering Journal*, vol. 100, pp. 182–207, Aug. 2024, ISSN: 1110-0168. DOI: 10.1016/j.aej.2024.05.030. [Online]. Available: https://www.sciencedirect.com/science/article/pii/S1110016824005003 (visited on 05/31/2024).

[6] J. Incer-Valverde, A. Korayem, G. Tsatsaronis, and T. Morosuk, ""Colors" of hydrogen: Definitions and carbon intensity," *Energy Conversion and Management*, vol. 291, p. 117 294, Sep. 2023, ISSN: 0196-8904. DOI: 10.1016/j.enconman.2023.117294. [Online]. Available: https://www.sciencedirect.com/science/article/pii/S0196890423006404 (visited on 05/31/2024).

[7] J. B. Heywood, *Internal Combustion Engine Fundamentals*, en, 2nd Edition. McGraw-Hill Education, 2018, ISBN: 9781260116106.

[8] S. Pischinger, *Lecture Notes Internal Combustion Engines*, 5th. RWTH Aachen University, 2012, vol. 1.

[9] G. Maio, A. Boberic, L. Giarracca, *et al.*, "Experimental and numerical investigation of a direct injection spark ignition hydrogen engine for heavy-duty applications," *International Journal of Hydrogen Energy*, vol. 47, no. 67, pp. 29 069–29 084, Aug. 2022, ISSN: 0360-3199. DOI: 10.1016/j.ijhydene.2022.06.184. [Online]. Available: https://www.sciencedirect.com/science/article/pii/S0360319922028208 (visited on 06/04/2024).

[10] G. M. R. Ryser M.Willmann and M. Gisigner, *Turbocharging and Synthetic Fuels*. MTZ worldwide, 2021, vol. 82. DOI: 10.1007/s38313-021-0641-3.

[11] S. R. Turns, *An Introduction to Combustion: Concepts and Applications*, en. McGraw-Hill Education, Jan. 2011, Google-Books-ID: RXSdcQAACAAJ, ISBN: 9780073380193.

[12] A. Wimmer, T. Wallner, J. Ringler, *et al.*, "H2-Direct Injection – A Highly Promising Combustion Concept," English, Apr. 2005, ISSN: 0148-7191, 2688-3627, 0148-7191, 2688-3627. DOI: 10.4271/2005-01-0108. [Online]. Available: https://saemobilus.sae.org/papers/h2-direct-injection-a-highly-promising-combustion-concept-2005-01-0108 (visited on 06/04/2024).

[13] K. Wittek, V. Cogo, and G. Prante, "Full load optimization of a hydrogen fuelled industrial engine," *International Journal of Hydrogen Energy*, vol. 77, pp. 230–243, Aug. 2024, ISSN: 0360-3199. DOI: 10.1016/j.ijhydene.2024.06.198. [Online]. Available: https://www.sciencedirect.com/science/article/pii/S0360319924024108 (visited on 06/18/2024).

[14] A. Paykani, H. Chehrmonavari, A. Tsolakis, T. Alger, W. F. Northrop, and R. D. Reitz, "Synthesis gas as a fuel for internal combustion engines in transportation," *Progress in Energy and Combustion Science*, vol. 90, p. 100 995, May 2022, ISSN: 0360-1285. DOI: 10.1016/j.pecs.2022.100995. [Online]. Available: https://www.sciencedirect.com/science/article/pii/S0360128522000041 (visited on 06/05/2024).

[15] ETTES. "Syngas biomass genset projects." Accessed: 2024-06-05. (2012), [Online]. Available: https://www.ettesgenerator.com/syngas-biomass-generation-projects.html.

[16] M. Fiore, V. Magi, and A. Viggiano, "Internal combustion engines powered by syngas: A review," *Applied Energy*, vol. 276, p. 115 415, Oct. 2020, ISSN: 0306-2619. DOI: 10.1016/j.apenergy.2020.115415. [Online]. Available: https://www.sciencedirect.com/science/article/pii/S0306261920309272 (visited on 06/05/2024).

[17] F. Y. Hagos, A. R. A. Aziz, and S. A. Sulaiman, "Syngas (H2/CO) in a spark-ignition direct-injection engine. Part 1: Combustion, performance and emissions comparison with CNG," *International Journal of Hydrogen Energy*, vol. 39, no. 31, pp. 17 884–17 895, Oct. 2014, ISSN: 0360-3199. DOI: 10.1016/j.ijhydene.2014.08.141.

[Online]. Available: https://www.sciencedirect.com/science/article/pii/S0360319914024823 (visited on 06/05/2024).

[18] R. Lechner, A. Hornung, and M. Brautsch, "Prediction of the knock propensity of biogenous fuel gases: Application of the detonation theory to syngas blends," *Fuel*, vol. 267, p. 117 243, May 2020, ISSN: 0016-2361. DOI: 10.1016/j.fuel.2020.117243. [Online]. Available: https://www.sciencedirect.com/science/article/pii/S0016236120302386 (visited on 06/06/2024).

[19] A. S. Bika, "Synthesis gas use in internal combustion engines.," en_US, Ph.D. dissertation, Dec. 2010. [Online]. Available: http://purl.umn.edu/99436 (visited on 06/10/2024).

[20] A. Langer, *A gas blending system*, eng. Feb. 1947, vol. 18, pp. 101–103. DOI: 10.1063/1.1740891.

[21] Bronkhorst. "What is thermal mass flow measurement?" Accessed: 2024-06-14. (2020), [Online]. Available: https://www.bronkhorst.com/int/service-support-1/technologies/thermal-mass-flow-measurement/.

[22] F. Ma, Y. Wang, J. Wang, *et al.*, "Development and Validation of an On-line Hydrogen-Natural Gas Mixing System for Internal Combustion Engine Testing," English, Jun. 2008, ISSN: 0148-7191, 2688-3627. DOI: 10.4271/2008-01-1580. [Online]. Available: https://www.sae.org/publications/technical-papers/content/2008-01-1580/ (visited on 06/14/2024).

[23] P. M. Gerhart, A. L. Gerhart, and J. I. Hochstein, *Munson, Young, and Okiishi's Fundamentals of FluidMechanics*, en. Willey, 2018. [Online]. Available: https://www.wiley.com/en-us/Munson%2C+Young+and+Okiishi's+Fundamentals+of+Fluid+Mechanics%2C+8th+Edition-p-9781119547990 (visited on 06/17/2024).

[24] W. Bohl and W. Elmendorf, *Technische Strömungslehre*, de-DE, 15th, V. Buchverlag, Ed. 2014, ISBN: 978-3-8343-3329-2. [Online]. Available: https://vogel-fachbuch.de/Technische-Stroemungslehre/978-3-8343-3329-2.B-book (visited on 06/14/2024).

[25] P. Coelho, *Tabelas de Termodinâmica*, 4th, L. E. Técnicas, Ed. 2017, ISBN: 978-989-752-262-8.

[26] WK-ARMATUREN. "Manufaktur für gassysteme armaturen." Accessed: 2024-06-14. (2024), [Online]. Available: https://wk-armaturen.de/.

[27] M. Co-Ax. Accessed: 2024-06-14. (2024), [Online]. Available: https://co-ax.com/en/.

[28] Cantera. Accessed: 2024-07-02. (2024), [Online]. Available: https://cantera.org/.

[29] V. Schröder, "Calculation of Flammability and Lower Flammability Limits of Gas Mixtures for Classification Purposes," 2016. [Online]. Available: https://www.semanticscholar.org/paper/Calculation-of-Flammability-and-Lower-Flammability-Schr%C3%B6der/0fbf244f19ea4efd2d9feeb95cedbb1a4abc1154 (visited on 07/03/2024).

# Appendix A

# Syngas Composition

Table A.1: Volumetric Composition of 3 Syngases obtained from different feedstocks

| Gas | Straw 750 °C | Digestate 750 °C | Sewage Sludge 750 °C |
|---|---|---|---|
| $H_2$ | 28.9964 | 32.8687 | 44.0641 |
| $CO_2$ | 19.8008 | 21.0351 | 14.5829 |
| $CO$ | 21.4476 | 16.8519 | 18.4722 |
| $CH_4$ | 11.4922 | 9.6504 | 7.4390 |
| Ethen | 2.8262 | 2.4023 | 0.7135 |
| Propen | 0.5401 | 0.6633 | 0.2862 |
| Ethan | 0.8997 | 0.8410 | 0.4246 |
| Propan | 0.0618 | 0.0774 | 0.0418 |
| $H_2S$ | 0.0000 | 0.2172 | 0.5399 |
| 1-Buten | 0.0137 | 0.0204 | 0.0057 |
| Butan | 0.0000 | 0.0000 | 0.0000 |
| 1-Penten | 0.0000 | 0.0000 | 0.0000 |
| Pentan | 0.0032 | 0.0022 | 0.0046 |
| 1-Hexen | 0.1410 | 0.1723 | 0.0857 |
| Hexan | 0.0253 | 0.0398 | 0.0011 |
| 1-Hepten | 0.3337 | 0.3275 | 0.2430 |
| Heptan | 0.0042 | 0.0032 | 0.0059 |
| Difference | 0.0042 | 0.0032 | 0.0059 |

## Appendix B

# P&ID Plan

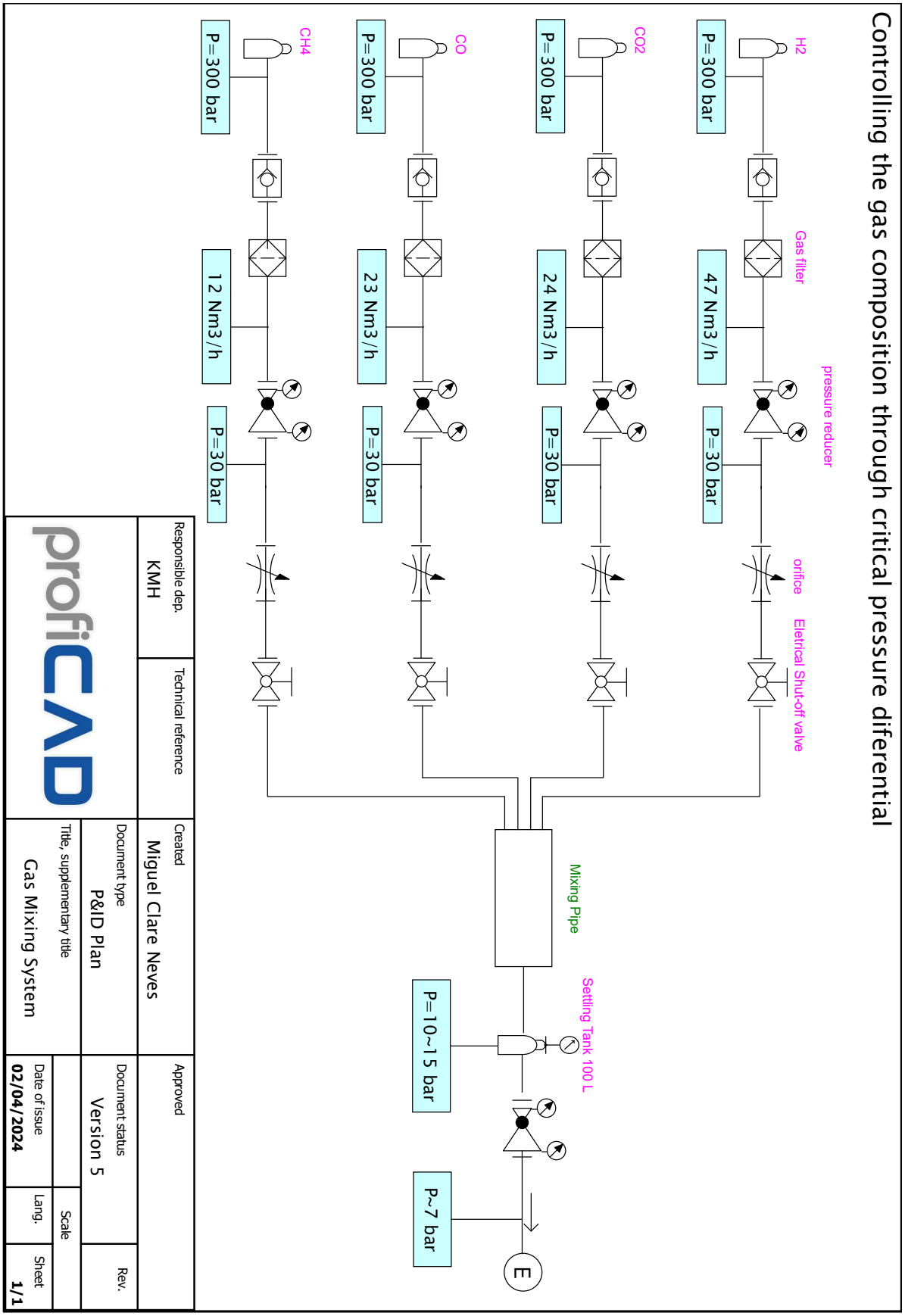
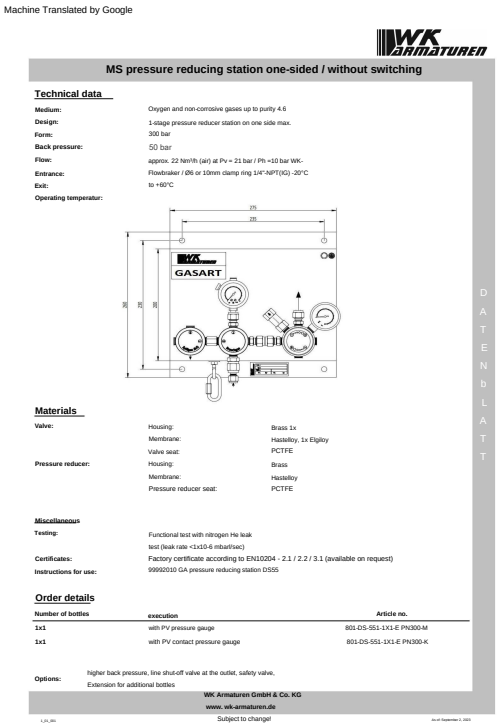



Figure B.1: Gas Mixing System P&ID plan

# Appendix C

# Components Data Sheets

## C.1 Pressure Regulator



Machine Translated by Google

**MS pressure reducing station one-sided / without switching**

**Technical data**

| | |
|---|---|
| **Medium:** | Oxygen and non-corrosive gases up to purity 4.6 |
| **Design:** | 1-stage pressure reducer station on one side max. |
| **Form:** | 300 bar |
| **Back pressure:** | 50 bar |
| **Flow:** | approx. 22 Nm³/h (air) at Pv = 21 bar / Pn =10 bar WK- |
| **Entrance:** | Flowbraker / Ø6 or 10mm clamp ring 1/4"-NPT(IG) -20°C |
| **Exit:** | to +60°C |
| **Operating temperatur:** | |



**Materials**

| | | |
|---|---|---|
| **Valve:** | Housing: | Brass 1x |
| | Membrane: | Hastelloy, 1x Elgiloy |
| | Valve seat: | PCTFE |
| **Pressure reducer:** | Housing: | Brass |
| | Membrane: | Hastelloy |
| | Pressure reducer seat: | PCTFE |

**Miscellaneous**

| | |
|---|---|
| **Testing:** | Functional test with nitrogen He leak test (leak rate <1x10-6 mbar*l/sec) |
| **Certificates:** | Factory certificate according to EN10204 - 2.1 / 2.2 / 3.1 (available on request) |
| **Instructions for use:** | 99992010 GA pressure reducing station DS55 |

**Order details**

| Number of bottles | execution | Article no. |
|---|---|---|
| 1x1 | with PV pressure gauge | 801-DS-551-1X1-E PN300-M |
| 1x1 | with PV contact pressure gauge | 801-DS-551-1X1-E PN300-K |

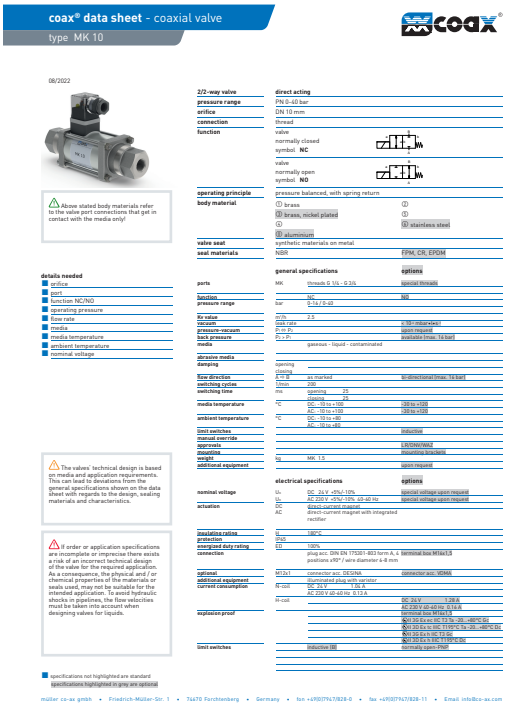
**Options:** higher back pressure, line shut-off valve at the outlet, safety valve, Extension for additional bottles

**WK Armaturen GmbH & Co. KG**
**www. wk-armaturen.de**
Subject to change!

DATENBLATT

Figure C.1: Pressure Reducer Specifications

## C.2 Shut-Off Valve



coax® data sheet – coaxial valve

type MK 10

08/2022

Above stated body materials refer to the valve port connections that get in contact with the media only!

details needed

- orifice
- port
- function NC/NO
- operating pressure
- flow rate
- media
- media temperature
- ambient temperature
- nominal voltage

The valves' technical design is based on media and application requirements. This can lead to deviations from the general specifications shown on the data sheet with regards to the design, sealing materials and characteristics.

If order or application specifications are incomplete or imprecise there exists a risk of an incorrect technical design of the valve for the required application. As a consequence, the physical and / or chemical properties of the materials or seals used, may not be suitable for the intended application. To avoid hydraulic shocks in pipelines, the flow velocities must be taken into account when designing valves for liquids.

specifications not highlighted are standard
specifications highlighted in grey are optional

| | | | |
|---|---|---|---|
| 2/2-way valve | | direct acting | |
| pressure range | | PN 0–60 bar | |
| orifice | | DN 10 mm | |
| connection | | thread | |
| function | | valve normally closed symbol **NC** | |
| | | valve normally open symbol **NO** | |
| operating principle | | pressure balanced, with spring return | |
| body material | | ① brass<br>② brass, nickel plated<br>③<br>④ aluminium | ①<br>①<br>③ stainless steel |
| valve seat | | synthetic materials on metal | |
| seal materials | | NBR | FPM, CR, EPDM |
| | | **general specifications** | **options** |
| ports | MK | threads G 1/4 – G 3/4 | special threads |
| function | | NC | NO |
| pressure range | bar | 0–7 / 0–10 | |
| Kv-value | m³/h | 2.5 | |
| flow rate | m³/h | | ≤ 10× nitrogen/air/ |
| pressure-vacuum | P→P₂ | | upon request |
| back pressure | P₂ > P→ | | available (max. 16 bar) |
| media | | gaseous – liquid – contaminated | |
| abrasive media | | | |
| damping | opening<br>closing | | |
| flow direction | ↓ or ⇓ | as marked | bi-directional (max. 16 bar) |
| switching cycles | l/min | 200 | |
| switching time | ms | opening 25<br>closing 25 | |
| media temperature | °C | DC: –10 to +100<br>AC: –10 to +150 | –20 to +120<br>–30 to +120 |
| ambient temperature | °C | DC: –10 to +80<br>AC: –10 to +60 | |
| limit switches | | | inductive |
| manual override | | | |
| approvals | | | LR/DNV/WAZ |
| mounting | | | mounting brackets |
| weight | kg | MK 1.5 | |
| additional equipment | | | upon request |
| | | **electrical specifications** | **options** |
| nominal voltage | $U_n$ | DC 24 V +5%/-10% | special voltage upon request |
| | $U_n$ | AC 220 V +5%/-10% 49–60 Hz | special voltage upon request |
| actuation | DC | direct-current magnet | |
| | AC | direct-current magnet with integrated rectifier | |
| insulating ratios | ti | 180°C | |
| protection | IP65 | | |
| energized duty rating | ED | 100% | |
| connection | | plug acc. DIN EN 175301-803 form A, 4 positions x90° / wire diameter 4–8 mm | terminal box M16x1.5 |
| optional | M12x1 | connector acc. DESINA | connector acc. VDMA |
| additional equipment | | illuminated plug with varistor | |
| current consumption | R-coil: | DC 24 V 1.04 A<br>AC 220 V 40–60 Hz 0.13 A | |
| | M-coil: | | DC 24 V 1.29 A<br>AC 230 V 40–60 Hz 0.16 A |
| explosion proof | | | terminal box M16x1.5<br>⟨Ex⟩ II 3G Ex ec IIC T3 Ta –20…+80°C Gc<br>⟨Ex⟩ II 2G Ex ic IIC T195°C Ta –20…+80°C Gb<br>⟨Ex⟩ II 3G Ex h IIC T3 Gc<br>⟨Ex⟩ II 3D Ex h IIIC T195°C Dc |
| limit switches | | inductive (S) | normally open (PNP) |

müller co-ax gmbh • Friedrich-Müller-Str. 1 • 74670 Forchtenberg • Germany • fon +49(0)7947/828-0 • fax +49(0)7947/828-11 • Email: info@co-ax.com

Figure C.2: Shut-Off Valve Specifications

# Appendix D

# Cantera Open-Source Codes

## D.1 Cantera open-source code to calculate Adiabatic Flame Temperature

```
from pathlib import Path
import cantera as ct
import numpy as np
import sys
import csv
import time


T = 300.0
P = 101325.0

gas = ct.Solution('gri30.yaml')
mix_phases = [(gas, 1.0)]
gas_copy = ct.Solution('gri30.yaml')
gas_flame = ct.Solution('gri30.yaml')

gas_name = 'H2'
fuel = 'H2:1, CO2:0, CO:0, CH4:0'


```

```
22
23 # equivalence ratio range
24 npoints = 15
25
26
27 AF = np.array([0.1,0.2,0.3,0.4, 0.5,0.6, 0.7,0.8,0.9, 1, 1.25,
       1.5,2,3,4])
28 phi = 1/AF
29
30 pressure = np.full(npoints, P)
31
32
33
34
35 # create some arrays to hold the data
36 tad = np.zeros(npoints)
37
38 tav = np.zeros(npoints)
39
40 flamespeed = np.zeros(npoints)
41
42
43 #Adiabatic Temperature variation with phi
44 for i in range(npoints):
45     # set the gas state
46
47     gas.set_equivalence_ratio(phi[i], fuel, 'O2:1.0, N2:3.76')
48
49     # create a mixture of 1 mole of gas.
50     mix = ct.Mixture(mix_phases)
51     mix.T = T
52     mix.P = P
53
54     # equilibrate the mixture adiabatically at constant P
55     mix.equilibrate('HP', solver='gibbs', max_steps=1000)
56
57     tad[i] = mix.T
58     #Average temperature
59     tav[i]=(gas.T+T)/2
60
61     print('At phi = {0:12.4g}, Tad = {1:12.4g}'.format(phi[i], tad
           [i]))
```

## D.2 Cantera open-source code to calculate Laminar Flame Speed

```
T = 300.0\\
P = 101325.0\\
gas = ct.Solution('gri30.yaml')\\
mix_phases = [(gas, 1.0)]\\
gas_copy = ct.Solution('gri30.yaml')\\
gas_flame = ct.Solution('gri30.yaml')\\

gas_name = 'H2'\\
fuel = 'H2:1, CO2:0, CO:0, CH4:0'\\




# equivalence ratio range\\
npoints = 15\\


AF = np.array([0.1,0.2,0.3,0.4,0.5,0.6, 0.7,0.8,0.9, 1, 1.25,
    1.5,2,3,4])\\
phi = 1/AF\\

pressure = np.full(npoints, P)\\


# create some arrays to hold the data\\
tad = np.zeros(npoints)\\

flamespeed = np.zeros(npoints)\\
#Laminar flame speed\\
width = 0.03 # m\\
loglevel = 1\\

for i in range(npoints):\\
    # Set the equivalence ratio\\
    gas.set_equivalence_ratio(phi[i], fuel, 'O2:1.0, N2:3.76')\\
    gas.TP = T, P\\

    # Create the FreeFlame object\\
    f = ct.FreeFlame(gas, width=width)\\
    f.set_refine_criteria(ratio=3, slope=0.06, curve=0.12)\\

    # Solve with mixture-averaged transport model\\
    f.transport_model = 'mixture-averaged'\\
    f.solve(loglevel=loglevel, auto=True)\\

    # Save the solution\\
```

```
46      if "native" in ct.hdf_support():\\
47          output = Path() / "adiabatic_flame.h5"\\
48      else:
49          output = Path() / "adiabatic_flame.yaml"\\
50      output.unlink(missing_ok=True)\\
51      f.save(output, name="mix", description="solution with mixture-
            averaged transport")\\
52
53      # Print mixture-averaged flamespeed\\
54      print(f"mixture-averaged flamespeed = {f.velocity[0]:7f} m/s")
            \\
55
56      # Solve with multi-component transport properties\\
57      f.transport_model = 'multicomponent'\\
58      f.solve(loglevel)  # don't use 'auto' on subsequent solves\\
59
60      # Print multicomponent flamespeed\\
61      print(f"multicomponent flamespeed = {f.velocity[0]:7f} m/s")\\
62
63      # Calculate and save other properties\\
64      flamespeed[i] = f.velocity[0]\\
65      print("\033[93m{}\033[0m".format(i))\\
```

## D.3 *EES* Code to Calculate Gas Properties

```
x_h2=0,195\\
x_co2=0,338\\
x_co=0,353\\
x_ch4=0,114\\
stoich =2,5552\\
m_fuel= 26,97[Kg/kmol]\\

"Calculations"\\
MW_fuel = molarmass(H2)*x_h2+molarmass(CO2)*x_co2+molarmass(CO)*
    x_co+molarmass(CH4)*x_ch4\\
 MW_mixture = molarmass(Air)*x_air+MW_fuel*x_fuel\\
m_h2 = x_h2 * molarmass(H2)\\
m_co2=x_co2*molarmass(CO2)\\
m_co=x_co*molarmass(CO)\\
m_ch4=x_ch4*molarmass(CH4)\\
R=8314/MW_mixture\\
rho= 101325/(R*T)\\



y_h2= m_h2/m_fuel\\
y_co2= m_co2/m_fuel\\
y_co= m_co/m_fuel\\
y_ch4= m_ch4/m_fuel\\
cp_fuel = cp(H2; T=T)*y_h2 + cp(CO2; T=T)*y_co2 + cp(CO; T=T)*y_co
     + cp(CH4; T=T)*y_ch4\\
k_fuel=conductivity(H2;T=T)*y_h2+conductivity(CO2;T=T)*y_co2+
    conductivity(CO;T=T)*y_co+conductivity(CH4;T=T)*y_ch4\\

 frac_h2=x_h2/(x_air+x_fuel)\\
 frac_co2=x_co2/(x_air+x_fuel)\\
 frac_co=x_co/(x_air+x_fuel)\\
 frac_ch4=x_ch4/(x_air+x_fuel)\\


m_air = lambda*stoich*MW_fuel\\

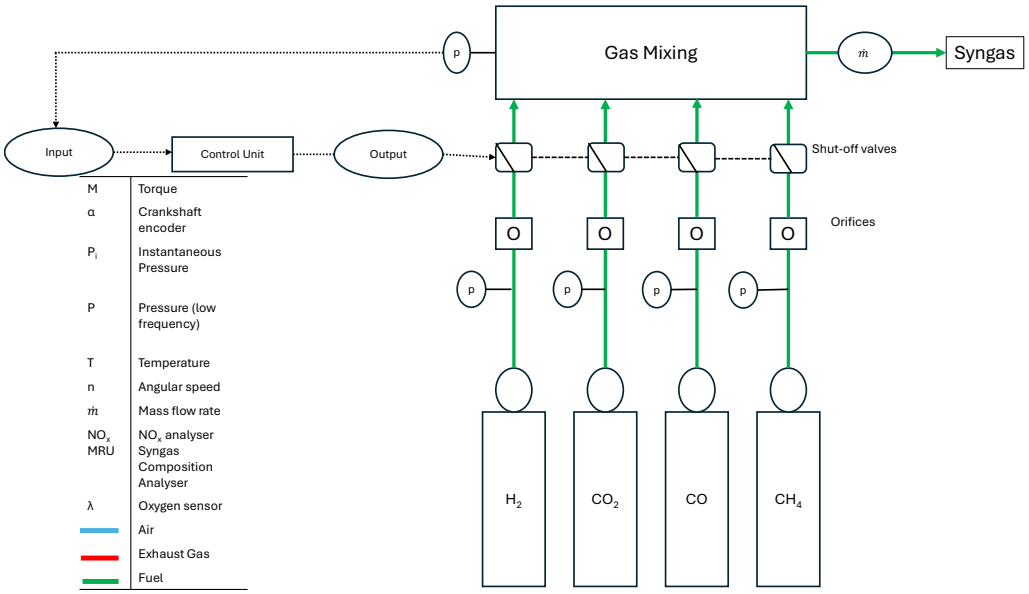

y_fuel = m_fuel/(m_air+m_fuel)\\
y_air = m_air/(m_air+m_fuel)\\
P=101325\\
n_fuel=m_fuel/MW_fuel\\
n_air=m_air/molarmass(Air)\\

x_air=(m_air/molarmass(Air))/(m_air/molarmass(Air)+m_fuel/MW_fuel)
    \\
```

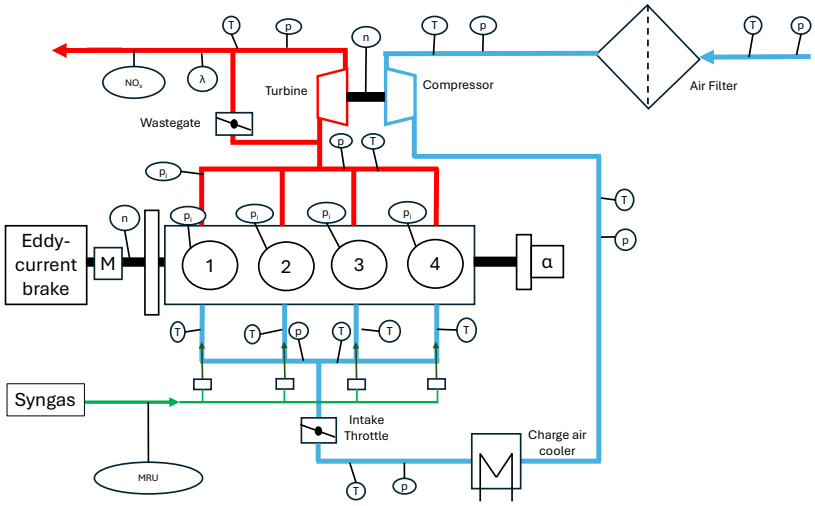
```
43 x_fuel=(m_fuel/MW_fuel)/(m_air/molarmass(Air)+m_fuel/MW_fuel)\\
44
45 cp_mix=cp_fuel * y_fuel + cp(Air;T=T)*y_air\\
46 k_mix = conductivity(Air;T=T)*y_air + k_fuel*y_fuel\\
```

## Appendix E

# ICE and Gas Mixing System Layout




(a) Gas Mixing System.




(b) ICE.

Figure E.1: Gas Mixing System and ICE Layout.

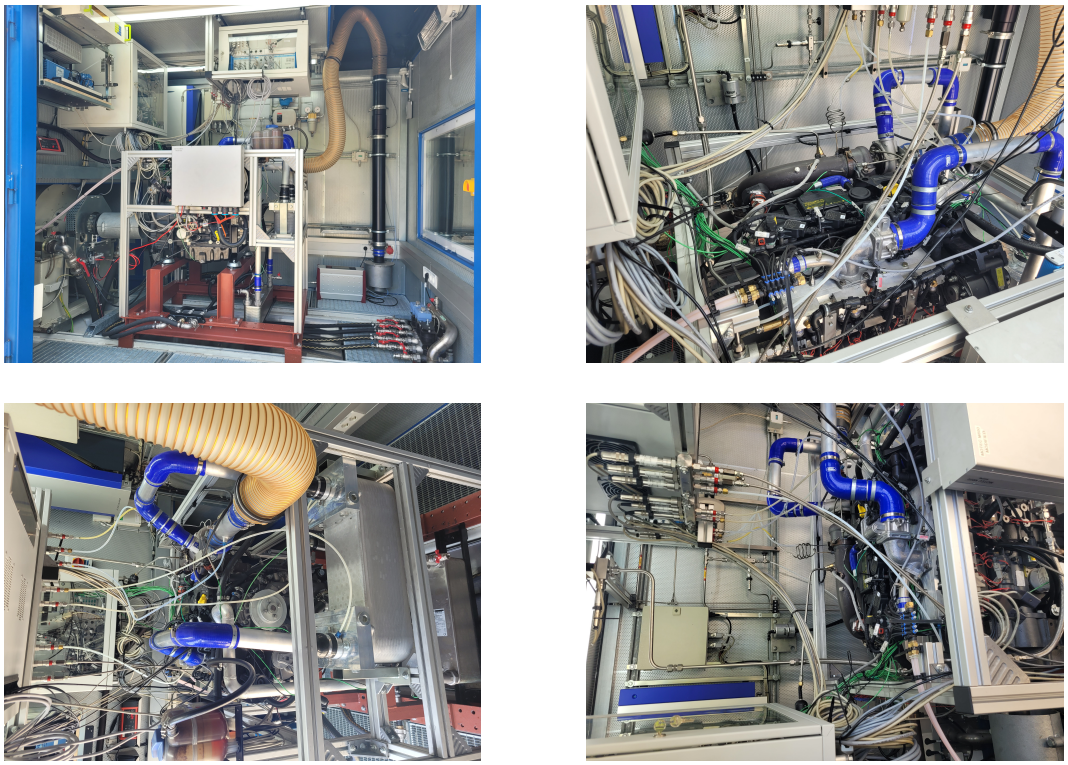


Figure E.2: ICE mounted in the test cell.



Figure E.3: Orifices and device used to test and calculate the Cd.